Q. J. R. Meteorol. Soc. (1991), **117**, pp. 685–714 551.515.21

An analytic theory of tropical-cyclone motion in a barotropic shear flow

By ROGER K. SMITH
Meteorological Institute, University of Munich, Federal Republic of Germany

(Received 16 October 1990; revised 20 May 1991)

SUMMARY

The recent analytic theory for the barotropic motion of an initially symmetric vortex on a beta plane at rest presented by Smith and Ulrich is extended to the case of a horizontal shear flow, enabling the precise effects of shear on vortex motion to be isolated. These effects are characterized by the contribution of the shear-related terms in the vorticity equation to the evolution and structure of the wave-number-1 component of the vortex asymmetry. The analysis proceeds on the assumption that a general shear flow may be adequately approximated by the first three terms of a double Taylor-series expansion about the initial vortex centre. The manner in which the linear and quadratic terms of this expansion affect the asymmetries is illustrated in detail for a zonal shear flow with a linear or quadratic variation in the meridional direction.

For tropical-cyclone-scale vortices, the theory shows excellent agreement with equivalent numerical calculations for a period of one or two days. As well as providing insight into the effects of horizontal shear on tropical-cyclone motion, the calculations have the potential to assist in the design of 'bogus' vortices for the initialization of dynamically based tropical-cyclone forecast models.

1. INTRODUCTION

Our current understanding of the dynamics of tropical-cyclone motion has evolved largely from numerical studies of barotropic vortex motion on a beta plane. The archetypal problem considers the initial-value problem for the motion of an initially symmetric vortex on a beta plane with zero basic flow (Anthes and Hoke 1975; Kitade 1981; Chan and Williams 1987; Fiorino and Elsberry 1989a, b; Shapiro and Ooyama 1990; Smith *et al.*, 1990), or with a zonal shear flow (DeMaria 1985, 1987; Shapiro and Ooyama 1990; Ulrich and Smith 1991). Ulrich and Smith op. cit. studied motion in a zonally varying basic flow also.

These studies have highlighted the role of vortex asymmetries which have the form of a pair of counter-rotating gyres, the so-called beta gyres. The gyres are generated by the advection of basic-state absolute vorticity by the vortex circulation. The numerical calculations have shown that the subsequent vortex motion can be associated with the total ambient flow (the basic flow plus the flow associated with the vortex-induced asymmetries) across the vortex centre.

The early analytic theory of Sasaki and Miyakoda (1954), Sasaki (1955) and Kasahara (1957, 1960), the latter for a baroclinic model, are essentially linear theories for the initial vortex motion and do not explain the motion found in numerical-model simulations where nonlinear effects are dominant (Chan and Williams 1987). The more recent study of Holland (1983) appears also to fit into this category. A more complete, partially analytic, theory which accounted for the interaction between the vortex and its environmental flow was worked out by Kasahara and Platzman (1963). These authors also gave a clear exposition of the problem of partitioning the flow between 'vortex' and 'environment', showing that there was no unique way of doing this. Other analytic studies are those of Willoughby (1989), Carr and Williams (1989), Peng and Williams (1991) and Smith and Ulrich (1990; henceforth denoted by SU). In the latter an approximate analytic theory was presented for the prototype initial-value problem, i.e. the motion of an initially symmetric vortex on a beta plane with zero basic flow. For a tropical-cyclone-scale vortex, the theory showed excellent agreement with the corresponding numerical calculation.

In the present paper the theory of SU is extended to the general initial-value problem of vortex motion in a shear flow, again on a beta plane. The availability of an analytic solution enables the factors governing the evolution of the gyre structure to be precisely identified and ordered in importance. The solution provides also a deeper understanding of the numerical calculations of Ulrich and Smith (1991; henceforth denoted by US) with some of which detailed comparisons are made.

2. The equations of motion

The barotropic vorticity equation in a fixed frame of reference (x, y) on a rotating earth is

$$\frac{\partial \zeta_*}{\partial t} + \mathbf{u}_* \cdot \nabla(\zeta_* + f) = 0 \tag{2.1}$$

where $\mathbf{u}_*$ is the horizontal velocity vector, ζ_* is the vertical component of relative vorticity, f is the Coriolis parameter and t is the time.

We consider the motion of a symmetric vortex located initially at the origin $(0, 0)$ of these coordinates and having a tangential velocity distribution $V(|\mathbf{x}|)$ with corresponding vorticity distribution $\zeta_0(|\mathbf{x}|)$. The vortex is embedded in a basic shear flow $\mathbf{u}_* = \bar{\mathbf{u}}(\mathbf{x}, t)$ with vorticity $\bar{\Gamma}(\mathbf{x}, t)$. The motion is assumed to occur on a northern hemisphere beta plane in which f increases linearly in the poleward direction y.

As in SU, we adopt the Kasahara–Platzman method of partitioning the flow between the 'vortex' and the 'environment' in which the vortex is defined as the initial vorticity distribution $\zeta(|\mathbf{x}|)$ suitably relocated, and the environment is defined as the residual vorticity field (i.e. that of the basic flow together with the vortex-induced distortion to it). Following SU, we define the vortex centre $\mathbf{x}_c = (x_c, y_c)$ to be the location of the relative-vorticity maximum.

We investigate the vortex motion and subsequent evolution of the vorticity field in a frame of reference (X, Y) translating with the vortex centre at velocity $\mathbf{c}$. In this frame, the vortex will continue to be defined as the vorticity distribution $\zeta(|\mathbf{X}|)$, with associated tangential wind speed denoted by $\mathbf{u}(|\mathbf{X}|) = (\mathbf{k} \wedge \hat{\mathbf{X}})V(|\mathbf{X}|)$, where $\hat{\mathbf{X}} = \mathbf{X}/|\mathbf{X}|$. The environmental flow will be defined as $\bar{\mathbf{U}} + \mathbf{U}_a$, where $\bar{\mathbf{U}}(\mathbf{X}, t) = \bar{\mathbf{u}}(\mathbf{x}, t)$ denotes the basic flow and $\mathbf{U}_a(\mathbf{X}, t)$ is the residual flow characterizing the vortex-induced asymmetries. The relative-vorticity fields corresponding with $\bar{\mathbf{U}}$ and $\mathbf{U}_a$ are $\bar{\Gamma}$ and Γ_a, respectively. In terms of these quantities, Eq. (2.1) can be written in the translating frame as

$$\frac{\partial}{\partial t}(\bar{\Gamma} + \Gamma_a + \zeta) + (\bar{\mathbf{U}} + \mathbf{U}_a + \mathbf{u}) \cdot \nabla(\bar{\Gamma} + \Gamma_a + \zeta + f) = -\mathbf{c} \cdot \nabla f. \tag{2.2}$$

By definition the basic flow is taken to be independent of the vortex, whereupon in the translating frame it satisfies the equation

$$\frac{\partial \bar{\Gamma}}{\partial t} + \bar{\mathbf{U}} \cdot \nabla(\bar{\Gamma} + f) = -\mathbf{c} \cdot \nabla f. \tag{2.3}$$

Also by definition the vortex trivially satisfies

$$\frac{\partial \zeta}{\partial t} + \mathbf{u} \cdot \nabla \zeta = 0. \tag{2.4}$$

Then subtracting Eqs. (2.3) and (2.4) from Eq. (2.2) we obtain an equation governing the evolution of the asymmetric vorticity

$$\frac{\partial \Gamma_a}{\partial t} + \mathbf{u} \cdot \nabla(\Gamma_a + \bar{\Gamma} + f) = -\bar{\mathbf{U}} \cdot \nabla(\Gamma_a + \zeta) - \mathbf{U}_a \cdot \nabla(\Gamma_a + \zeta + \bar{\Gamma} + f). \tag{2.5}$$

Note the term on the right-hand side of Eq. (2.3) represents the rate of change of absolute vorticity associated with the rate of change of latitude of the coordinate system. It leads to a spatially uniform particular integral $\bar{\Gamma}_f = -\beta y_c$ of the equation, where $\beta = df/dy$. It turns out to be convenient later to associate this term with the asymmetric vorticity and to assume that $\bar{\Gamma}$ satisfies Eq. (2.3) with zero right-hand side.

In the following sections we consider approximate solutions to this equation for a steady basic flow $\bar{\mathbf{u}}(x, y)$ of the form

$$\begin{aligned}\bar{\mathbf{u}}(x, y) &= \{\bar{u}(x, y), \bar{v}(x, y)\} \\ &= \bar{\mathbf{u}}_0 + \mathbf{x} \cdot \nabla \bar{\mathbf{u}}_0 + \tfrac{1}{2}x^2 \frac{\partial^2 \bar{\mathbf{u}}_0}{\partial x^2} + xy \frac{\partial^2 \bar{\mathbf{u}}_0}{\partial x \partial y} + \tfrac{1}{2}y^2 \frac{\partial^2 \bar{\mathbf{u}}_0}{\partial y^2}\end{aligned} \tag{2.6}$$

where a subscript '0' denotes evaluation at the origin of the fixed frame (recall that this is the initial vortex position).

Let the vortex position at time t be $\mathbf{x}_c = (x_c, y_c)$. Then $d\mathbf{x}_c/dt = \mathbf{c}$. In SU, where there was no basic flow, we adopted the closure assumption that $\mathbf{U}_a(0, 0) = 0$, i.e. the relative velocity of the asymmetric flow across the vortex centre is zero, the condition that determines $\mathbf{c}$. The validity of this assumption was confirmed in numerical simulations by Smith *et al.* (1990). The series of numerical calculations of vortex motion in spatially varying basic flows by US show that, to a very good approximation, the vortex-centre velocity as defined here is equal to the total environmental flow across the vortex centre, i.e.

$$\mathbf{c} = \bar{\mathbf{U}}(0, 0) + \mathbf{c}_a \tag{2.7}$$

where $\mathbf{c}_a$ is determined again by the condition that $\mathbf{U}_a(0, 0) = 0$. Accordingly we adopt this as our closure assumption in the present theory.

Substituting $\mathbf{x} = \mathbf{x}_c + \mathbf{X}$ in Eq. (2.6) and noting that $\bar{\mathbf{U}}(0, 0) = \bar{\mathbf{u}}(x_c, y_c)$, we obtain

$$\begin{aligned}\bar{\mathbf{U}}(X, Y) = \bar{\mathbf{U}}(0, 0) + (\mathbf{X} + \mathbf{x}_c) \cdot \nabla \bar{\mathbf{U}}_0 + \tfrac{1}{2}X(X + 2x_c) \frac{\partial^2 \bar{\mathbf{u}}_0}{\partial x^2} + \\ + (XY + x_c Y + y_c X) \frac{\partial^2 \bar{\mathbf{u}}_0}{\partial x \partial y} + \tfrac{1}{2}Y(Y + 2y_c) \frac{\partial^2 \bar{\mathbf{u}}_0}{\partial y^2}.\end{aligned} \tag{2.8}$$

Since $\nabla_x = \nabla_X$, the relative vorticity of the basic state, $\bar{\Gamma} = \mathbf{k} \cdot \nabla_X \wedge \bar{\mathbf{U}}$, is given by

$$\bar{\Gamma} = \bar{\Gamma}_0 + \mathbf{X} \cdot \nabla_x \bar{\Gamma}_0 + \mathbf{x}_c \cdot \nabla_x \bar{\Gamma}_0 \tag{2.9}$$

and the absolute vorticity thereof is

$$\bar{\Gamma}_{abs} = \bar{\Gamma}_0 + f_0 + AX + BY + O(|\mathbf{x}_c|) \tag{2.10}$$

where

$$(A, B) = (\partial \bar{\Gamma}_0/\partial x, \beta + \partial \bar{\Gamma}_0/\partial y). \tag{2.11}$$

3. Zero-order calculation of $\mathbf{U}_a(\mathbf{X})$

As in SU we assume that, to a first approximation, the vortex asymmetry is associated solely with the advection of basic-state absolute vorticity by the symmetric vortex

circulation; this has tangential wind speed $V(r) = r\Omega(r)$, $\Omega(r)$ being the angular rotation rate of the vortex. This assumption is equivalent to solving Eq. (2.5) with the right-hand side equal to zero, but the calculation is perhaps easier to carry out by reference to Fig. 1.

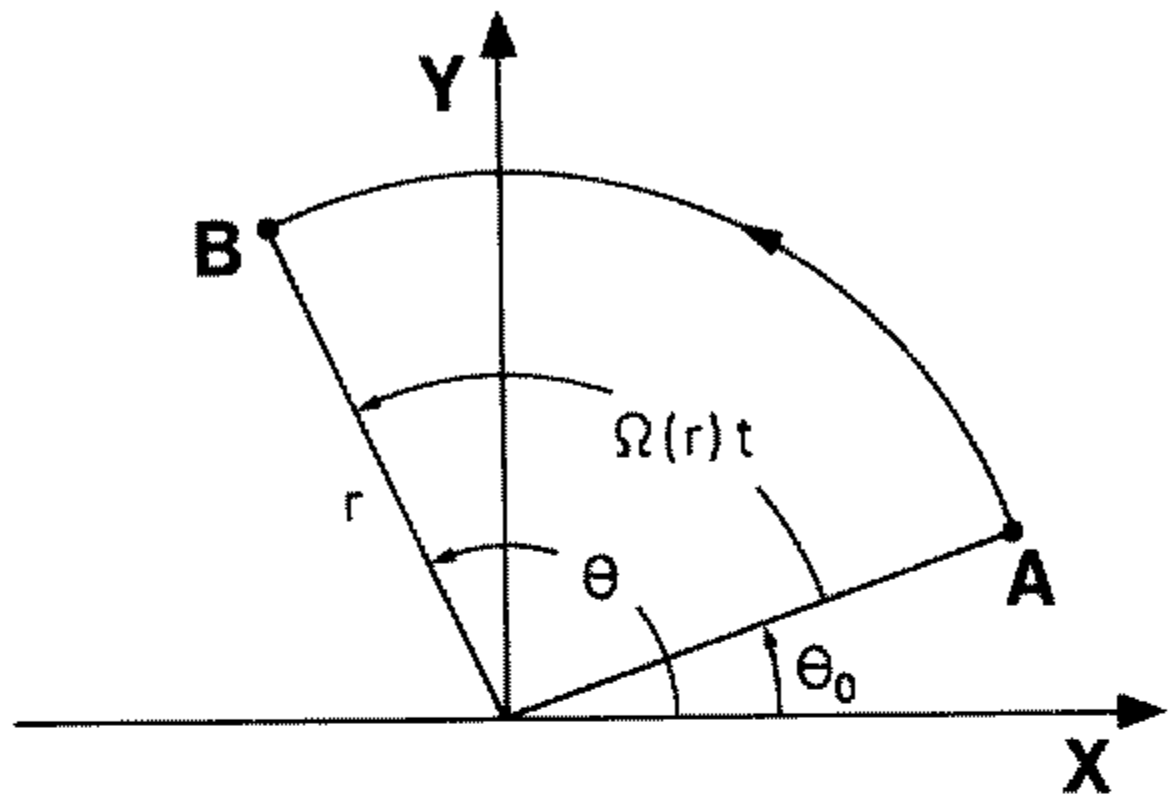

Figure 1. Arc of a hypothetical air-parcel trajectory, AB, circulating about the moving vortex centre. To calculate $\Gamma_a(r, \theta, t)$ in Eq. (3.3) it is assumed that the air parcel moves along the arc of a circle of radius r with angular velocity $\Omega(r)$.

Consider an air parcel initially at the point A with polar coordinates (r, θ_0) and absolute vorticity $\overline{\Gamma}_{\text{abs A}}$. If this moves anticlockwise to the point B(r, θ) along an arc of the circle with radius r in time t, conserving its absolute vorticity, then the asymmetric vorticity at B, Γ_{aB}, equals $-(\overline{\Gamma}_{\text{absB}} - \overline{\Gamma}_{\text{absA}})$, since Γ_a is initially zero. Using Eq. (2.10) and neglecting for the present the contribution of $O(|\mathbf{x}_c|)$, it follows that

$$\Gamma_a(r, \theta) = -Ar(\cos\theta - \cos\theta_0) - Br(\sin\theta - \sin\theta_0) \tag{3.1}$$

and since

$$\theta = \theta_0 + \Omega(r)t \tag{3.2}$$

this reduces with a little algebra to the form

$$\Gamma_0(r, \theta, t) = \zeta_1(r, t)\cos\overline{\theta} + \zeta_2(r, t)\sin\overline{\theta} \tag{3.3}$$

where

$$\zeta_1(r, t) = -B_* r \sin\{\Omega(r)t\} \tag{3.4a}$$

$$\zeta_2(r, t) = -B_* r[1 - \cos\{\Omega(r)t\}] \tag{3.4b}$$

$$B_* = \sqrt{(\overline{A^2 + B^2})} \tag{3.5a}$$

and

$$\overline{\theta} = \theta + \tan^{-1}(A/B) = \theta + \theta_*, \text{ say.} \tag{3.5b}$$

Here and in what follows we use the suffix '0' instead of 'a' to denote the zero-order vortex asymmetry. Comparing expressions (3.3) and (3.4) with Eqs. (2.6) and (2.7) of SU we note that an east–west gradient of $\overline{\Gamma}$ leads to a clockwise rotation of the zero-order vorticity asymmetry about an angle θ_* as well as to an increase in the strength of the asymmetry through the contribution to B_* in Eq. (3.5a).

The zero-order stream-function asymmetry satisfies $\nabla^2\Psi_0 = \Gamma_0$, together with the boundary condition $\Psi_0 \to \Psi_c(t)$ as $r \to \infty$, where

$$\Psi_c(t) = r\{-c_2(t)\cos\theta + c_1(t)\sin\theta\} \tag{3.6}$$

is the stream function associated with a uniform flow equal and opposite to the vortex translation (relative) velocity $\mathbf{c}_a$. Thus Ψ_c represents the relative asymmetric flow at large distances from the vortex on account of the vortex motion. As in SU, it follows readily that

$$\Psi_0(r, \theta, t) = \psi_1(r, t) \cos \overline{\theta} + \psi_2(r, t) \sin \overline{\theta} \tag{3.7}$$

where for $n = 1, 2$

$$\psi_n(r, t) = \tfrac{1}{2} r \int_0^r \left(1 - \frac{p^2}{r^2}\right) \zeta_n(p, t)\, dp. \tag{3.8}$$

The form of Eq. (3.7) implies a choice of $c_1(t)$, $c_2(t)$ in Eq. (3.6) to ensure that the corresponding *relative* velocity (U_0, V_0) is identically zero at the vortex centre, and this choice represents the implementation of the closure assumption at zero order. It may be shown that

$$\begin{bmatrix} c_1 \\ c_2 \end{bmatrix} = \begin{bmatrix} f_2(t) & f_1(t) \\ -f_1(t) & f_2(t) \end{bmatrix} \begin{bmatrix} \cos \theta_* \\ \sin \theta_* \end{bmatrix} \tag{3.9}$$

where

$$f_n(t) = \tfrac{1}{2} r \int_0^\infty \zeta_n(p, t)\, dp, \ (n = 1, 2). \tag{3.10}$$

The relative-velocity field (U_0, V_0) is given by

$$U_0 = -\frac{\partial \Psi_0}{\partial Y} = -\sin \theta \frac{\partial \Psi_0}{\partial r} - \frac{\cos \theta}{r} \frac{\partial \Psi_0}{\partial \theta} \tag{3.11a}$$

and

$$V_0 = \frac{\partial \Psi_0}{\partial X} = \cos \theta \frac{\partial \Psi_0}{\partial r} - \frac{\sin \theta}{r} \frac{\partial \Psi_0}{\partial \theta} \tag{3.11b}$$

with Ψ_0 given by Eq. (3.7).

4. First-order correction to $\mathbf{U}_a(\mathbf{X})$

As shown in SU, in the absence of a basic flow, the zero-order theory captures the structure of the vortex asymmetries to a remarkable extent, but the agreement with the numerical simulations can be considerably improved by calculating a first-order correction, Γ_1, obtained by integrating Eq. (2.5) with the operator acting on Γ_1 on the left-hand side and Γ_0 from the zero-order theory (Eq. (3.3)) on the right-hand side. We shall show here that the same is true in the presence of a uniform and/or linear shear.

The equation for the first-order vorticity correction is

$$\frac{\partial \Gamma_1}{\partial t} + \mathbf{u} \cdot \nabla \Gamma_1 = -\mathbf{U}_0 \cdot \nabla \zeta - \mathbf{U}_0 \cdot \nabla(\overline{\Gamma} + f) - \mathbf{U}_0 \cdot \nabla \Gamma_0 - \overline{\mathbf{U}} \cdot \nabla \zeta - \overline{\mathbf{U}} \cdot \nabla \Gamma_0. \tag{4.1}$$

Since this is linear in Γ_1, we can consider the contributions to Γ_1 from each of the terms on the right-hand side separately. We denote these by Γ_{1n} $(n = 1\text{–}5)$.

(a) *Calculation of* Γ_{11}

Using Eqs. (3.7) and (3.11), it follows after a little algebra that

$$-\mathbf{U}_0 \cdot \nabla\zeta = (\Psi_2 \cos\overline{\theta} - \Psi_1 \sin\overline{\theta}) \frac{1}{r}\frac{d\zeta}{dr}. \tag{4.2}$$

The equation for the contribution Γ_{11},

$$\frac{\partial\Gamma_{11}}{\partial t} + \mathbf{u} \cdot \nabla\Gamma_{11} = -\mathbf{U}_0 \cdot \nabla\zeta \tag{4.3}$$

may be integrated to give

$$\Gamma_{11}(r, \theta, t) = \zeta_{11}(r, t) \cos\overline{\theta} + \zeta_{12}(r, t) \sin\overline{\theta} \tag{4.4}$$

where

$$\zeta_{1n}(r, t) = -\tfrac{1}{2}B_* \frac{d\zeta}{dr} \int_0^r p\left(1 - \frac{p^2}{r^2}\right) \eta_n(r, p, t)\, dp \tag{4.5}$$

and

$$\eta_1(r, p, t) = \frac{\sin\{\Omega(r)t\}}{\Omega(r)} - \frac{\sin\{\Omega(r)t\} - \sin\{\Omega(p)t\}}{\Omega(r) - \Omega(p)} \tag{4.6a}$$

$$\eta_2(r, p, t) = \frac{1 - \cos\{\Omega(r)t\}}{\Omega(r)} + \frac{\cos\{\Omega(r)t\} - \cos\{\Omega(p)t\}}{\Omega(r) - \Omega(p)}. \tag{4.6b}$$

The details are given in Appendix A of SU. The integrals in Eq. (4.5) may be readily evaluated using quadrature when $\Omega(r)$ is prescribed.

(b) *Calculation of* Γ_{12}

$$-\mathbf{U}_0 \cdot \nabla(\overline{\Gamma} + f) = \frac{1}{r} J(f + \overline{\Gamma}, \psi_1 \cos\overline{\theta} + \psi_2 \sin\overline{\theta})$$

where $J(a, b) = (\partial a/\partial r)(\partial b/\partial\theta) - (\partial b/\partial r)(\partial a/\partial\theta)$ is the Jacobian operator. With a little algebra it can be shown using Eq. (2.11) that $\partial(f + \overline{\Gamma})/\partial r = B_* \sin\overline{\theta}$ and $\partial(f + \overline{\Gamma})/\partial\theta = B_* r \cos\overline{\theta}$; and with some further reduction it is found that

$$-\mathbf{U}_0 \cdot \nabla(\overline{\Gamma} + f) = A_2(r, t) + B_2(r, t) \cos 2\overline{\theta} + C_2(r, t) \sin 2\overline{\theta} \tag{4.7}$$

where

$$\left.\begin{aligned} A_2 &= -\tfrac{1}{2}B_* \left(\frac{\partial\psi_1}{\partial r} + \frac{\psi_1}{r}\right) \\ B_2 &= -\tfrac{1}{2}B_* \left(\frac{\partial\psi_1}{\partial r} - \frac{\psi_1}{r}\right) \end{aligned}\right\} \tag{4.8}$$

and

$$C_2 = -\tfrac{1}{2}B_* \left(\frac{\partial\psi_2}{\partial r} - \frac{\psi_2}{r}\right).$$

Then using Eq. (3.8) with Eq. (3.4), the equation

$$\frac{\partial\Gamma_{12}}{\partial t} + \mathbf{u} \cdot \nabla\Gamma_{12} = -\mathbf{U}_0 \cdot \nabla(\overline{\Gamma} + f) \tag{4.9}$$

can be integrated to give

$$\Gamma_{12} = \zeta_{20}(r,t) + \zeta_{2c}(r,t)\cos 2\overline{\theta} + \zeta_{2s}(r,t)\sin 2\overline{\theta} \tag{4.10}$$

where the functional forms of $\zeta_{2\nu}(r,t)$, $(\nu = 0,c,s)$ and additional details of the calculation are given in Appendix 1.

(c) *Calculation of* Γ_{13}

$$-\mathbf{U}_0 \cdot \nabla\Gamma_0 = \frac{1}{r}J(\zeta_1 \cos\overline{\theta} + \zeta_2 \sin\overline{\theta}, \psi_1 \cos\overline{\theta} + \psi_2 \sin\overline{\theta})$$

reduces with a little algebra to a similar form to Eq. (4.7), i.e.

$$-\mathbf{U}_0 \cdot \nabla\Gamma_0 = A_3(r,t) + B_3(r,t)\cos 2\theta + C_3(r,t)\sin 2\theta. \tag{4.11}$$

Then, as in section 4(b), the equation

$$\frac{\partial\Gamma_{13}}{\partial t} + \mathbf{u}\cdot\nabla\Gamma_{13} = -\mathbf{U}_0\cdot\nabla\Gamma_0 \tag{4.12}$$

can be integrated to give

$$\Gamma_{13} = \zeta_{30}(r,t) + \zeta_{3c}(r,t)\cos 2\overline{\theta} + \zeta_{3s}(r,t)\sin 2\overline{\theta}. \tag{4.13}$$

Again the details, including expressions for $\zeta_{3\nu}(r,t)$, $(\nu = 0,c,s)$, are sketched in Appendix 1.

(d) *Calculation of* Γ_{14}

For a basic flow of the form of Eqs. (2.6) or (2.8) it is convenient to introduce the deformation terms $E_0 = U_{x0} - V_{y0}$, $F_0 = V_{x0} + U_{y0}$ and their gradients evaluated at the origin, in addition to the vorticity $\Gamma_0 \equiv V_{x0} - U_{y0}$. Of course, the divergence and its derivatives must be zero in this model. Then with some straightforward algebraic manipulation the term $\overline{\mathbf{U}}\cdot\nabla\zeta$ may be written in the form

$$\begin{aligned}-\overline{\mathbf{U}}\cdot\nabla\zeta = {} & \tfrac{1}{8}r^2\frac{d\zeta}{dr}(\overline{\Gamma}_{y0}\cos\theta - \overline{\Gamma}_{x0}\sin\theta) - \tfrac{1}{2}r\frac{d\zeta}{dr}(E_0\cos 2\theta - F_0\sin 2\theta) - \\ & - \tfrac{1}{8}r^2\frac{d\zeta}{dr}\{(E_{x0} - F_{y0})\cos 3\theta + (E_{y0} + F_{x0})\sin 3\theta\} - \\ & - \tfrac{1}{2}r\frac{d\zeta}{dr}x_c(E_{x0}\cos 2\theta + F_{x0}\sin 2\theta) - \\ & - \tfrac{1}{2}r\frac{d\zeta}{dr}y_c(E_{y0}\cos 2\theta + F_{y0}\sin 2\theta).\end{aligned} \tag{4.14}$$

Let Γ_{14i} $(i = 1\text{–}4)$ denote the contributions to the solution of

$$\frac{\partial\Gamma_{14}}{\partial t} + \mathbf{u}\cdot\nabla\Gamma_{14} = -\overline{\mathbf{U}}_0\cdot\nabla\zeta \tag{4.15}$$

from the first, second, third and the sum of the last two terms on the right-hand side of Eq. (4.14). Then, as detailed in Appendix 2,

$$\Gamma_{141} = \zeta_{41c}(r,t)\cos\theta + \zeta_{41s}(r,t)\sin\theta \tag{4.16a}$$

$$\Gamma_{142} = \zeta_{42c}(r,t)\cos 2\theta + \zeta_{42s}(r,t)\sin 2\theta \tag{4.16b}$$

$$\Gamma_{143} = \zeta_{43c}(r,t)\cos 3\theta + \zeta_{43s}(r,t)\sin 3\theta \tag{4.16c}$$

and

$$\Gamma_{144} = \zeta_{44c}(r,t)\cos 2\theta + \zeta_{44s}(r,t)\sin 2\theta. \tag{4.16d}$$

For a general flow, the expressions for $\zeta_{44c}(r,t)$ and $\zeta_{44s}(r,t)$ are rather cumbersome and we have restricted attention to the case of a zonal shear flow. In particular, for uniform shear, only Γ_{142} is nonzero.

(e) *Calculation of* Γ_{15}

For a zonal shear flow $\overline{\mathbf{U}} = (\overline{U}(y), 0)$,

$$-\overline{\mathbf{U}}\cdot\nabla\Gamma_0 = \{\overline{\Gamma}_0 Y + \tfrac{1}{2}\overline{\Gamma}_{0y} Y(Y+2y_c)\}\frac{\partial\Gamma_0}{\partial X}. \tag{4.17}$$

If Γ_{15i} ($i = 1$–3) denote the contributions to the solution of

$$\frac{\partial\Gamma_{15}}{\partial t} + \mathbf{u}\cdot\nabla\Gamma_{15} = -\overline{\mathbf{U}}\cdot\nabla\Gamma_0 \tag{4.18}$$

from the terms proportional to Y, Y^2 and Yy_c on the right-hand side of Eq. (4.17), it can be shown that

$$\Gamma_{151} = \zeta_{51c}(r,t)\cos\theta + \zeta_{51s}(r,t)\sin\theta + \zeta_{51c3}(r,t)\cos 3\theta + \zeta_{51s3}(r,t)\sin 3\theta \tag{4.19a}$$

$$\Gamma_{152} = \zeta_{520}(r,t) + \zeta_{52c}(r,t)\cos 2\theta + \zeta_{52s}(r,t)\sin 2\theta + \zeta_{52c4}(r,t)\cos 4\theta + \zeta_{52s4}(r,t)\sin 4\theta \tag{4.19b}$$

$$\Gamma_{153} = \zeta_{53c}(r,t)\cos\theta + \zeta_{53s}(r,t)\sin\theta + \zeta_{53c3}(r,t)\cos 3\theta + \zeta_{53s3}(r,t)\sin 3\theta \tag{4.19c}$$

as detailed in Appendix 3. It is noteworthy that for a uniform shear, only Γ_{151} is nonzero as is evident from Eq. (4.17).

5. Gyre structure calculations

In this section we apply the foregoing theory to analyse the vorticity and stream-function asymmetries that develop in the course of motion of an initially symmetric vortex in uniform or linear shear. The initial vortex is the same as that used by Smith *et al.* (1990) and SU, having a maximum tangential wind speed of $40\,\mathrm{m\,s^{-1}}$ at a radius of 100 km and reducing to $15\,\mathrm{m\,s^{-1}}$ at 300 km radius. For later reference the corresponding radial vorticity profile is shown in Fig. 2. The results are compared with the numerical calculations of US. Accordingly, unless otherwise stated, the standard value of β used is $2.23\times10^{-11}\,\mathrm{m^{-1}\,s^{-1}}$ which we denote by β_{st}. To begin with we consider aspects of the calculation for zero basic flow that were not addressed in SU.

(a) *Zero basic flow*

The theory presented in SU considered the contribution of the vorticity correction Γ_{11}, but only briefly that of Γ_{12}, arguing that this, together with the contribution of Γ_{13}, should be small. This is confirmed by the present analysis as indicated in Fig. 3. The latter compares the asymmetric vorticity field $\Gamma_0 + \Gamma_{11}$ (Fig. 3(a)) as calculated by SU with the total field $\Gamma_0 + \Gamma_1$ (Fig. 3(b)). The most obvious difference is that the anticyclonic gyre is slightly stronger and the cyclonic gyre is slightly weaker in the total field, consistent with a symmetric anticyclonic vorticity contribution from Γ_{12} and Γ_{13}. Inclusion of the additional terms brings the asymmetry even closer to that calculated from the full numerical solution of the problem shown in Fig. 3(c) (see also SU, Fig. 10).

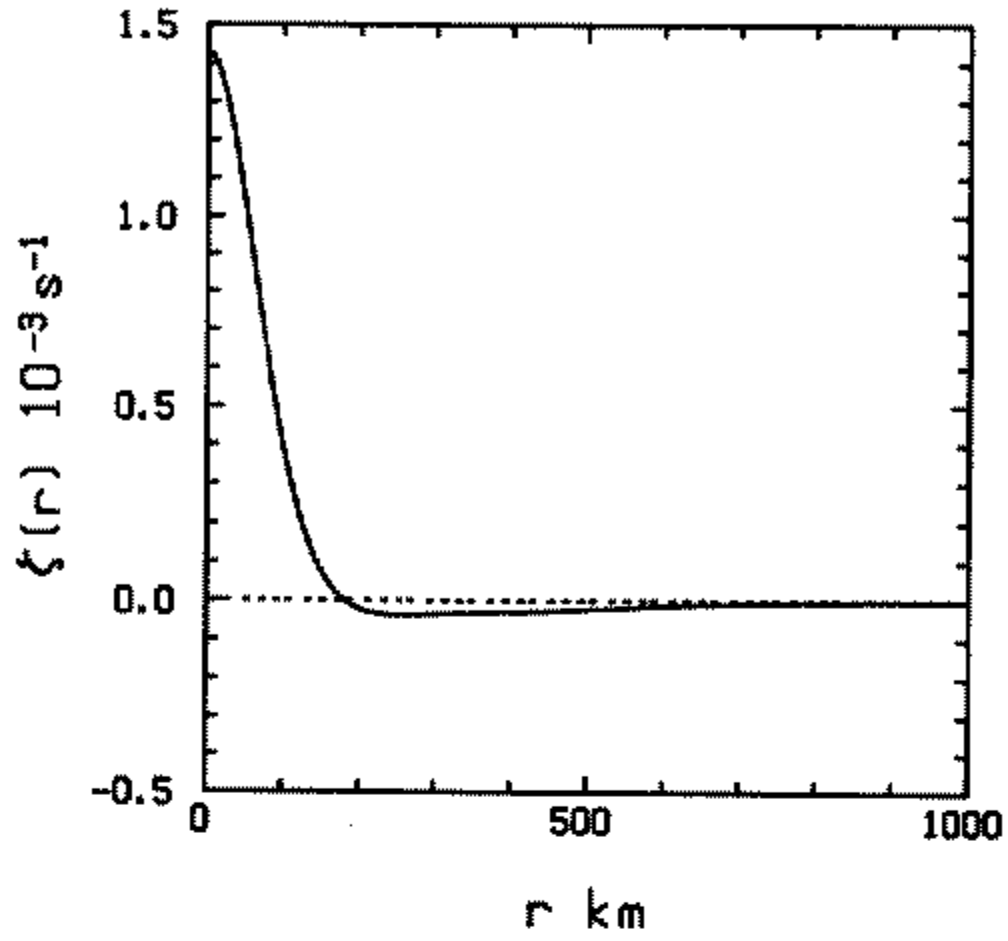

Figure 2. Radial profile of vortex vorticity, $\zeta(r)$, for the calculations presented in this paper.

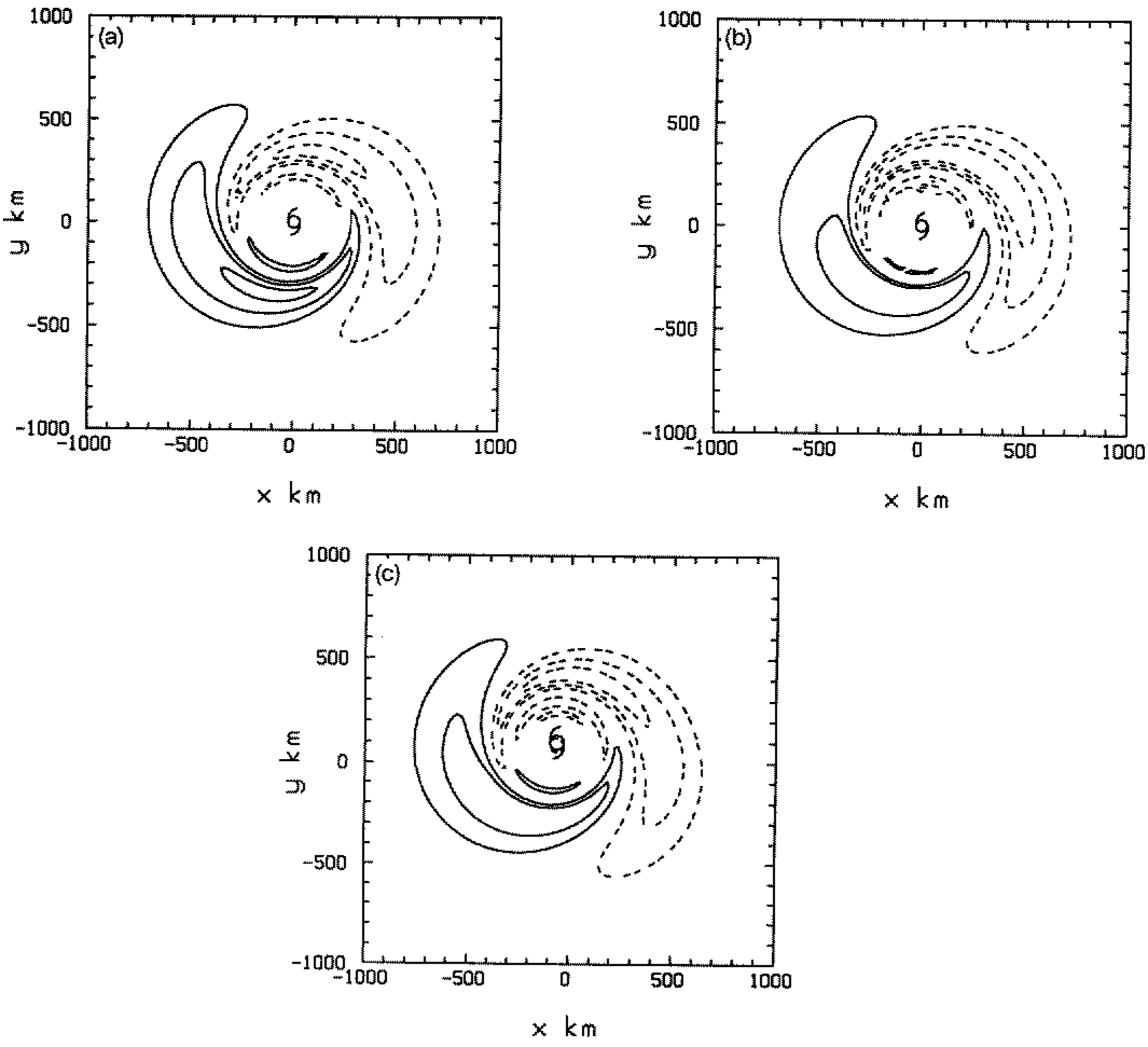

Figure 3. (a) Asymmetric vorticity field, $\Gamma_0 + \Gamma_{11}$, at 24 hours as calculated by SU, (b) the total field $\Gamma_0 + \Gamma_{11} + \Gamma_{12} + \Gamma_{13}$ and (c) the corresponding field obtained by Smith *et al.* (1990) from a full numerical solution of the problem. Contour interval is $5.0 \times 10^{-6} s^{-1}$. Dashed lines indicate negative values.

The symmetric contributions are of interest, *inter alia*, because they characterize changes to the total symmetric vortex circulation as the flow evolves; recall that these changes are considered as changes to the environment in the present method of partitioning. The symmetric vorticity corrections $\zeta_{20}(r,t)$† and $\zeta_{30}(r,t)$ and their sum are shown in Fig. 4(a) at 24 hours and the tangential velocity profile associated with their sum is shown in Fig. 4(b). Note that ζ_{20} is anticyclonic and relatively uniform inside a radius of 300 km beyond which it decreases rapidly to zero. In contrast, ζ_{30} has a narrow cyclonic regime between 250 and 450 km, peaking near 300 km with a value comparable in magnitude with the minimum value of ζ_{20}, and a broader anticyclonic regime with a minimum near 550 km radius. Accordingly, $\zeta_{20}+\zeta_{30}$ is everywhere anticyclonic. Its magnitude is relatively large and uniform to a radius of 250 km, beyond which it reduces rapidly to zero and then increases again to reach a second maximum near 550 km, reflecting the contribution from ζ_{30}. At larger radii its magnitude decreases rapidly to zero. The associated tangential velocity profile reflects the double-peak structure of the vorticity field; the velocity increases linearly with radius where the vorticity is appreciably uniform, starts to decay as the vorticity falls to zero, and then increases further to reach a maximum (in magnitude) of $0.23\,\mathrm{m\,s^{-1}}$ at 700 km. Beyond this radius the tangential wind speed steadily declines, albeit slowly, i.e. the finite anticyclonic circulation as $r\rightarrow\infty$ implies a decay like $1/r$ in the wind speed at sufficiently large radii. The particular form and size of this correction to the symmetric wind speed has implications for the ultimate breakdown of the analytic theory at large times (see section 7).

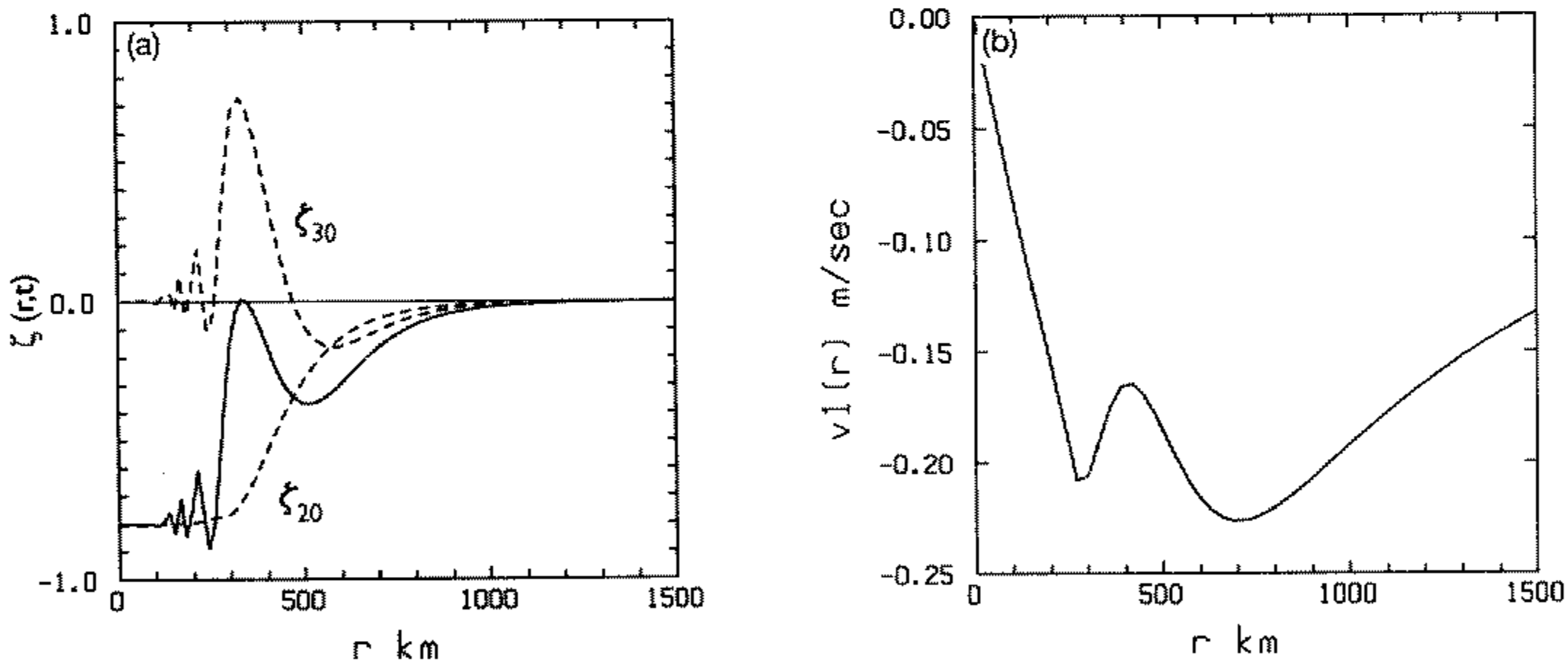

Figure 4. (a) Symmetric vorticity corrections $\zeta_{20}(r,t)$, $\zeta_{30}(r,t)$ and their sum (solid line) at 24 hours. (b) Radial profile of tangential velocity $v1(r)$ associated with the vorticity field $\zeta_{20}+\zeta_{30}$ at 24 hours.

(*b*) *Sheared basic flow*

In general, the effects of shear on the evolving vortex structure are two-fold. Firstly, shear acts to distort the existing vorticity field including the symmetric vortex, an effect represented by Γ_{14}, and the vorticity asymmetry, the distortion of which is characterized by the term Γ_{15}. For convenience we refer to these as the 'vortex distortion' and 'asymmetry distortion', respectively. Secondly, linear shear contributes to the basic-state absolute-vorticity gradient and thereby enhances or reduces the effect of beta, the source of vortex asymmetry in the case of zero basic flow.

† Actually, here and elsewhere, a uniform vorticity $\zeta_{20}(\infty,t)$ has been subtracted from $\zeta_{20}(r,t)$. As shown in Appendix 1, this represents the increase in basic-state absolute vorticity associated with the meridional motion of the vortex. Its inclusion would imply a solid-body rotation about the vortex centre.

(i) *Uniform shear.* For a linear velocity profile (i.e. for uniform shear), $\overline{\Gamma}_{0y} = 0$, so that the only contribution to Γ_{14} is from Γ_{142}. Thus uniform shear produces a wave-number-2 vortex distortion. This is easy to understand by reference to Fig. 5. The vortex vorticity gradient is negative inside a radius of 255 km (say r_0) and positive outside this radius (Fig. 2). Therefore $\partial\zeta/\partial X$ is positive for $X > 0$ and $r > r_0$ and negative for $X < 0$ and $r < r_0$. If $U = -\overline{U}_{0y}Y$, $-\overline{U}\,\partial\zeta/\partial X$ is negative in the first and third quadrants for $r > r_0$ and positive in the second and fourth quadrants. For $r < r_0$, the signs are reversed. Figure 6(a) shows the calculation of Γ_{14} at 24 hours when $\overline{U}_{0y} = 5\,\mathrm{m\,s^{-1}}$ per 1000 km, the case 3A2 studied by US and designated here as the case LP1 (for linear velocity profile, positive sign). Since the vorticity tendency is relative to the motion of a rotating air parcel (Eq. (4.1)), the pattern of Γ_{14} at inner radii is strongly influenced by the large radial shear of the azimuthal wind and consists of interleaving spiral regions of positive and negative vorticity. The maximum amplitude of Γ_{14} ($1.1 \times 10^{-5}\,\mathrm{s^{-1}}$ at 24 hours) occurs at a radius greater than r_0. Figures 6(b) and 6(c) show the corresponding contributions to Γ_{151} from wave-number 1 and wave-number 3 respectively (see Eq. (4.19)) which, for uniform shear, is the only nonzero contribution to the asymmetry distortion, Γ_{15}. Both contributions have maxima rather *less* than that of Γ_{14} ($3.2 \times 10^{-6}\,\mathrm{s^{-1}}$ and $2.2 \times 10^{-6}\,\mathrm{s^{-1}}$, respectively), but the former is important because asymmetries with wave-number 1 affect the vortex motion (see section 6).

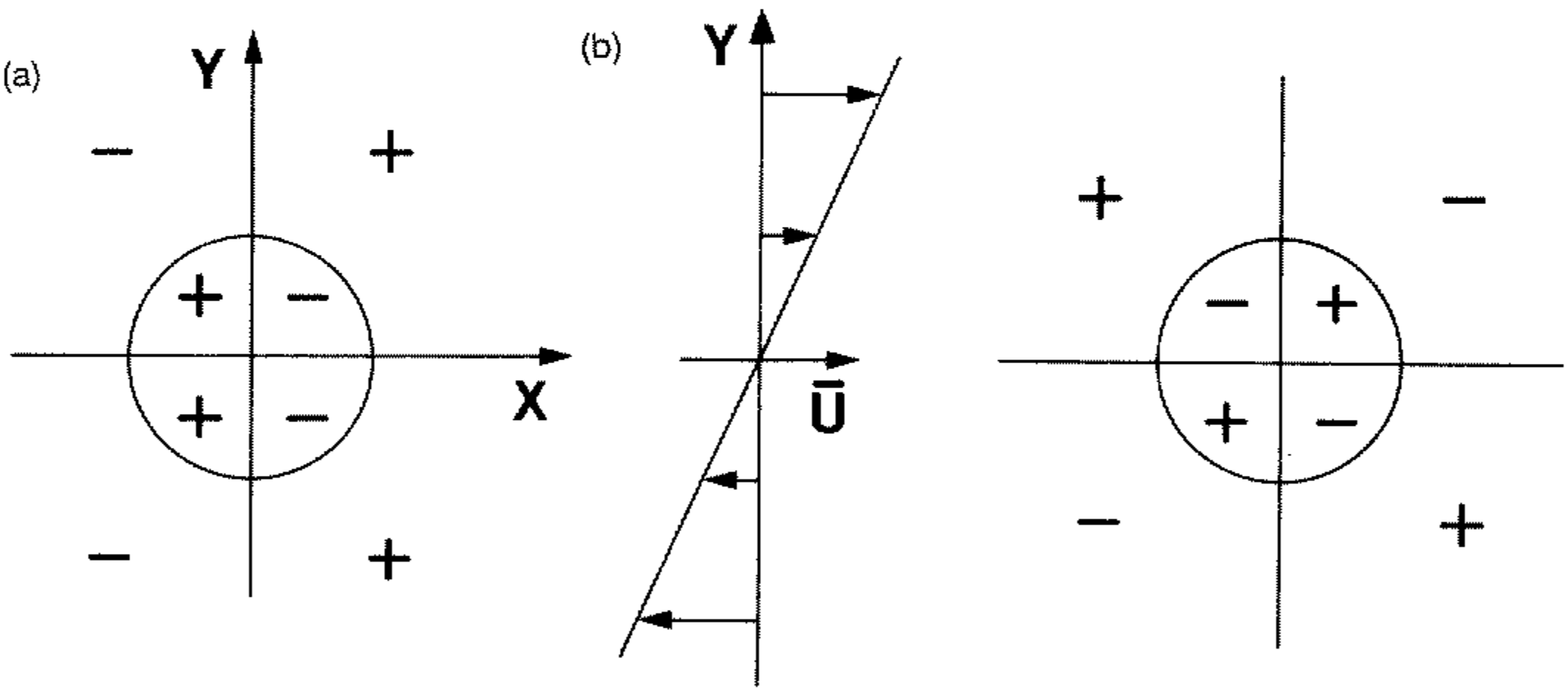

Figure 5. Schematic depiction of the wave-number-2 vorticity tendency arising from the term $-\overline{\mathbf{U}} \cdot \nabla\zeta = -\overline{U}\zeta_X$ in the case of a uniform basic shear $\overline{U} = U'Y$; (a) shows the sign of the vorticity gradient ζ_X in each quadrant for $0 < r < r_0$ and $r_0 < r$, where r_0 is the radius at which the vorticity gradient $d\zeta/dr$ changes sign (see Fig. 2) and (b) shows the vorticity tendency $-\overline{U}\zeta_X$ in the eight regions.

The total vorticity asymmetry at 24 hours for the case LP1 is shown in Fig. 7 where it is compared with the corresponding numerical calculation from US. Overall, the patterns are very similar, although there are minor differences in detail as indicated in Fig. 8(a). This shows the numerically calculated asymmetry relative to the vortex centre minus that calculated analytically. The main difference is represented by a pair of cyclonic gyres centred some 500 km north-east and south-west of the vortex centre. These are not significant in the sense that they appear to have little effect on the vortex track (see section 6). The comparison of the analytically with the numerically calculated asymmetry for the case of negative shear ($\overline{U}_{0y} = -5\,\mathrm{m\,s^{-1}}$ per 1000 km), the case 3A1 studied by US and designated here by LN, show also good agreement (cf. Figs. 7(c) and 7(d)). Again the main difference between the two fields is a pair of cyclonic rotating gyres, now

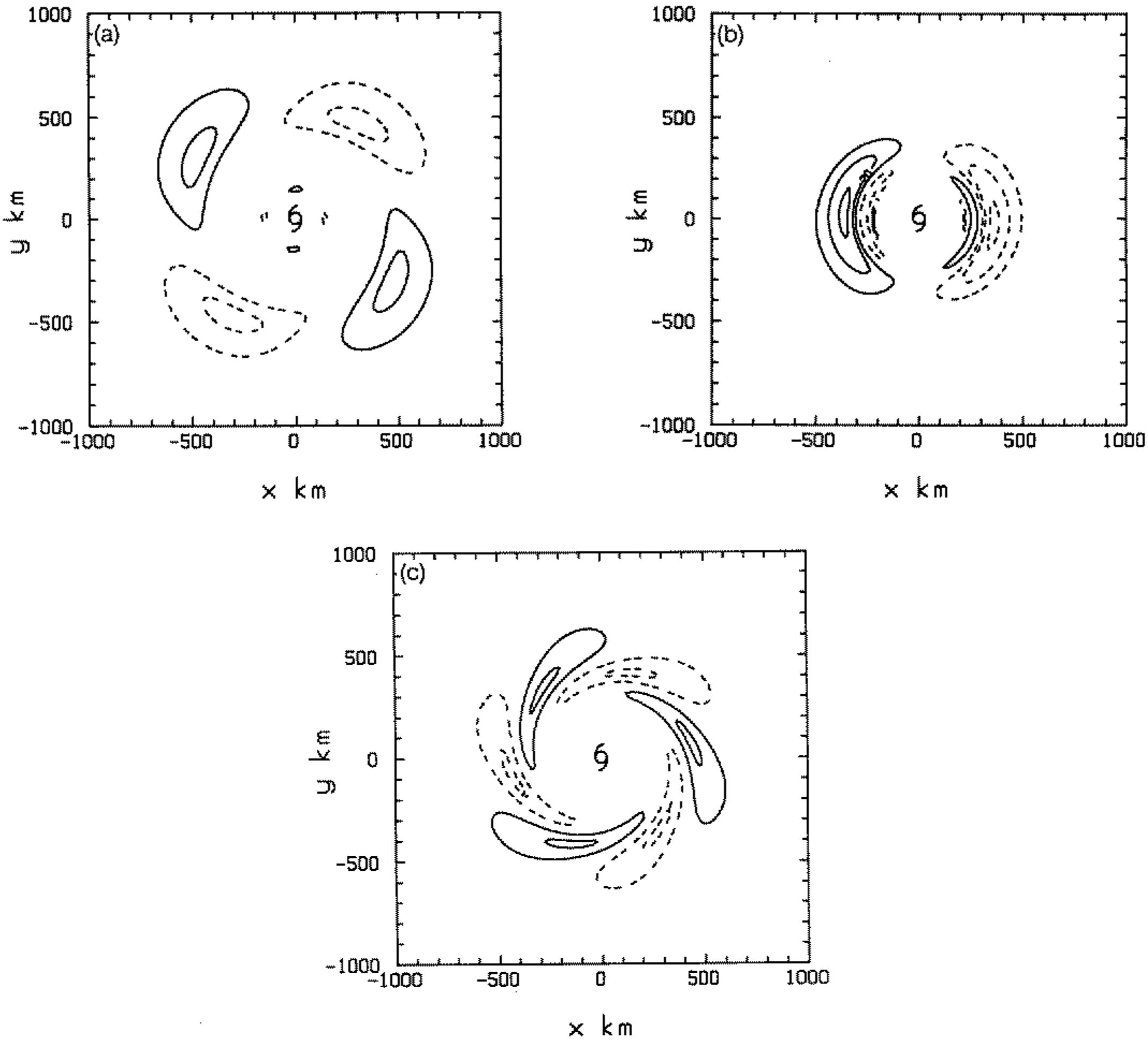

Figure 6. Asymmetric vorticity contributions (a) Γ_{14}, (b) the wave-number-1 contribution to Γ_{151}, and (c) the wave-number-3 contribution to Γ_{151}, for the case of a uniform basic shear with $\bar{U}_{0y} = 5\,\mathrm{m\,s^{-1}}$ per 1000 km at 24 hours. Contour interval is $5.0 \times 10^{-6}\,\mathrm{s^{-1}}$ in (a) and $1.0 \times 10^{-6}\,\mathrm{s^{-1}}$ in (b) and (c). Dashed lines indicate negative values. The vortex centre, marked by a cyclone symbol, is at the centre of each panel.

centred some 500 km north-west and south-east of the vortex centre (Fig. 8(b)). While these are a little stronger than in the previous case, they have little obvious effect on the vortex track.

As the shear is increased, the difference between the numerically and analytically calculated asymmetries begins to show a wave-number-2 component. This is exemplified by Fig. 8(c) which shows the difference field for case LP2, which is identical with LP1 except that the magnitude of the shear is twice as large, i.e. $10\,\mathrm{m\,s^{-1}}$ per 1000 km. One might surmize that this discrepancy could be reduced by including a vorticity correction in which the shear-induced asymmetry Γ_{14} is itself distorted by the shear. This does not appear to be the case, although the structure of the discrepancy suggests that it is caused by the progressive invalidity of the linearization about a circular vortex at large radial distances when calculating the zero order vortex asymmetry. This effect increases with time and increases with the magnitude of the shear.

Comparisons of the asymmetric stream function for the two cases LP1 and LN are made in section 5(c).

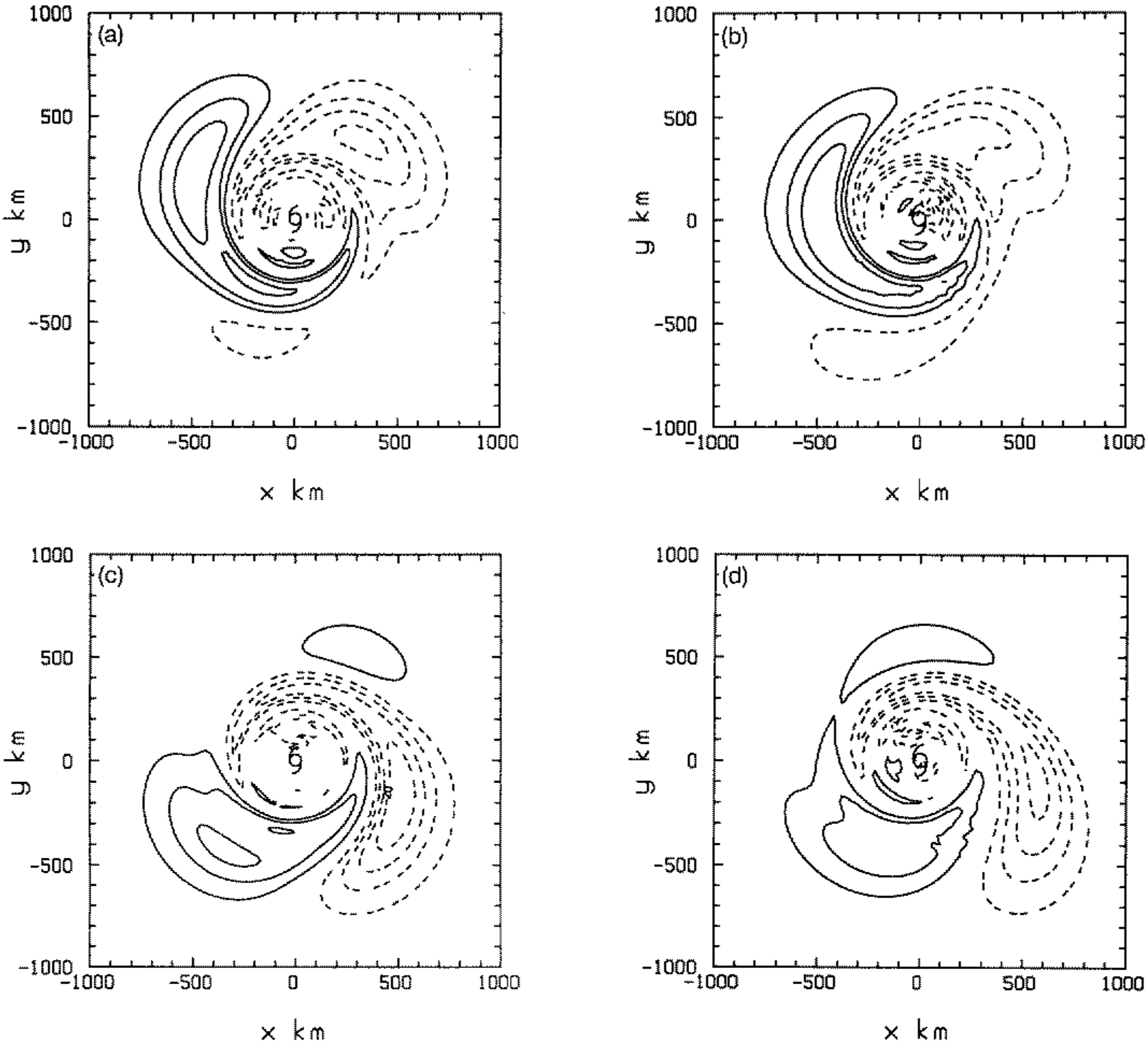

Figure 7. Total asymmetric vorticity field for the case of uniform basic shear in Fig. 6 at 24 hours. (a) Analytical calculation and (b) corresponding numerical calculation (case 3A2) of US. The corresponding comparisons for the case of negative shear ($\overline{U}_{0y} = -5\,\mathrm{m\,s^{-1}}$ per 1000 km; case 3A1 of US) are shown in (c) and (d). Contour interval in each case is $5.0 \times 10^{-6}\,\mathrm{s^{-1}}$. Dashed lines indicate negative values. The vortex centre, marked by a cyclone symbol, is at the centre of each panel.

(ii) *Linear shear.* We consider now the case of a quadratic velocity profile (i.e. linear shear) in which $\overline{U}_{y0}$ is taken to be zero (whereupon $\overline{\Gamma}_0 = 0$ and hence Γ_{142} and Γ_{151} are both zero), but $\overline{U}_{yy0}$, and therefore $\overline{\Gamma}_{y0}$, is nonzero. It follows that Γ_{14} has contributions from wave numbers 1, 2 and 3 while Γ_{15} has contributions from wave numbers 1–4 and from the symmetric term in Eq. (4.19(b)). Linear shear has two particularly important effects that lead to a wave-number-1 asymmetry, thereby affecting the vortex track. The first is characterized by the contribution to the absolute-vorticity gradient of the basic flow, which directly affects the zero-order vorticity asymmetry through its contribution to B (see Eq. (2.10)) and hence to B_*. The second is associated with the distortion of the vortex vorticity as depicted in Fig. 9 and represented mathematically by the term Γ_{141} (see Eq. (4.16(a))). This and the other contributions to Γ_{14} at 24 hours are shown in Fig. 10 for the case designated as SHB in which $\overline{\Gamma}_{y0} = \frac{1}{2}\beta_{st}$ and $\beta = \frac{1}{2}\beta_{st}$ (the case 3B1 studied by US).

For $\overline{\Gamma}_{y0} > 0$, the wave-number-1 asymmetry, Γ_{141}, is oriented so as to contribute a north-north-westerly component of flow across the vortex centre (Fig. 10(a)). As shown

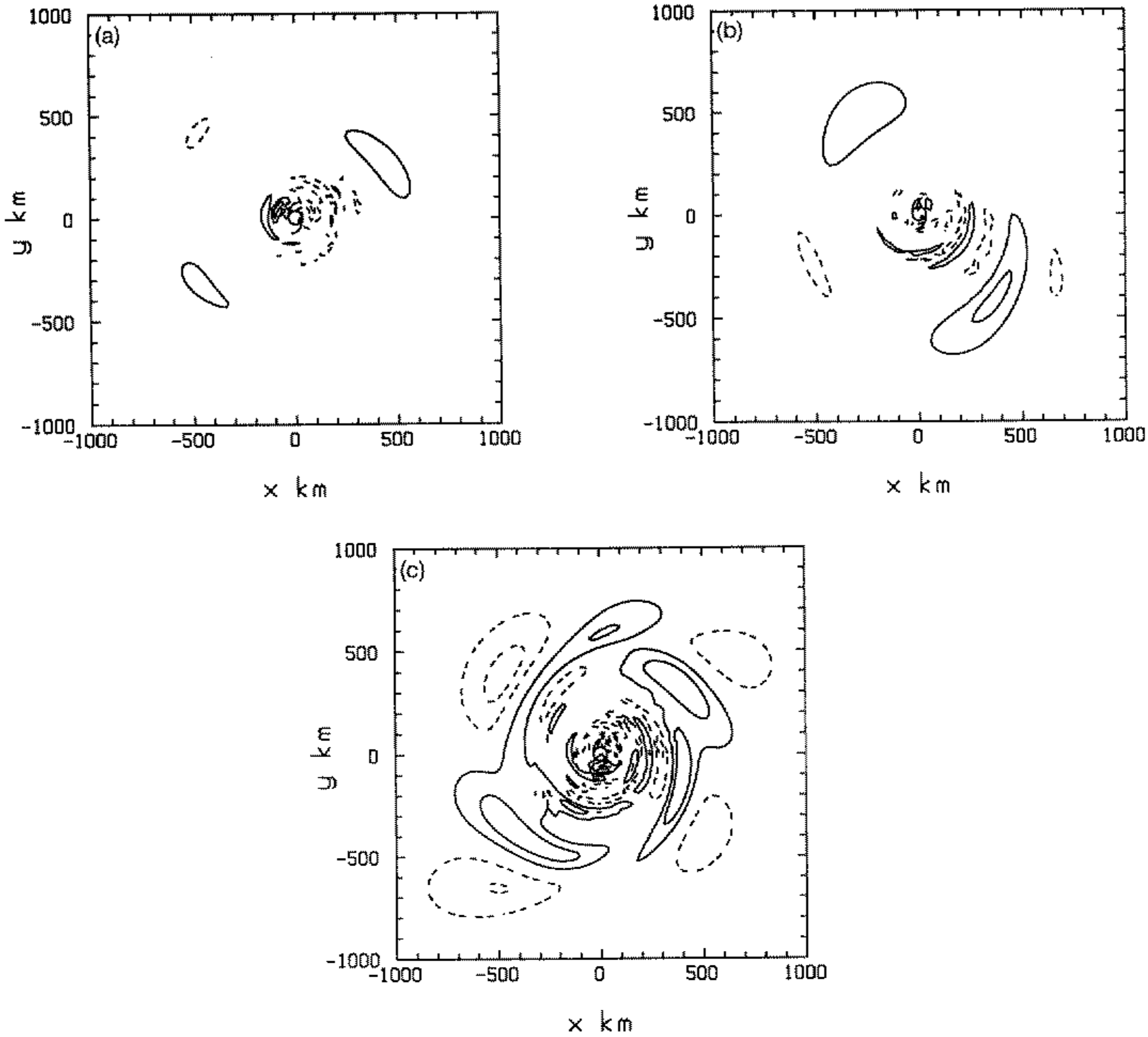

Figure 8. Difference between the numerically and analytically calculated vortex asymmetries (numerical minus analytic) at 24 hours for the uniform shear cases (a) LP1, (b) LN and (c) LP2 (see text for explanation). Contour interval is the same as in Fig. 7. Dashed lines indicate negative differences. The vortex centre, marked by a cyclone symbol, is at the centre of each panel.

in section 6, this has a significant effect on the vortex track. The maximum value of Γ_{141} at 24 hours is $3.8 \times 10^{-6}\,s^{-1}$. The wave-number-3 contribution to Γ_{14} (Γ_{143}) is comparable in magnitude (maximum value $3.6 \times 10^{-6}\,s^{-1}$), but neither this nor the wave-number-2 contribution (maximum value $8.0 \times 10^{-7}\,s^{-1}$) affects the vortex motion.

The differential advection of the zero-order vorticity asymmetry by a quadratic shear flow leads to the first-order correction Γ_{15}. The latter is relatively small compared with Γ_{14}, but it does include a wave-number-1 component that slightly affects the vortex track, as well as a predominantly anticyclonic symmetric contribution. The total symmetric component, $\zeta_{20} + \zeta_{30} + \zeta_{520}$, has a profile structure very similar to ζ_{30} in Fig. 4(a), but has a minimum of $1.8 \times 10^{-6}\,s^{-1}$. The wave-number-1 component of Γ_{15} is shown in Fig. 10(d) at 24 hours; it has a maximum at this time of $3.6 \times 10^{-7}\,s^{-1}$.

Figure 11 shows the total vorticity asymmetry at 24 hours for the case SHB, together with the corresponding asymmetry obtained from the numerical calculation in US. As in the case of uniform shear, the comparison is very good, the principal difference in detail being a weak elongated cyclonic anomaly some 600 km to the south-east of the vortex (Fig. 12(a)).

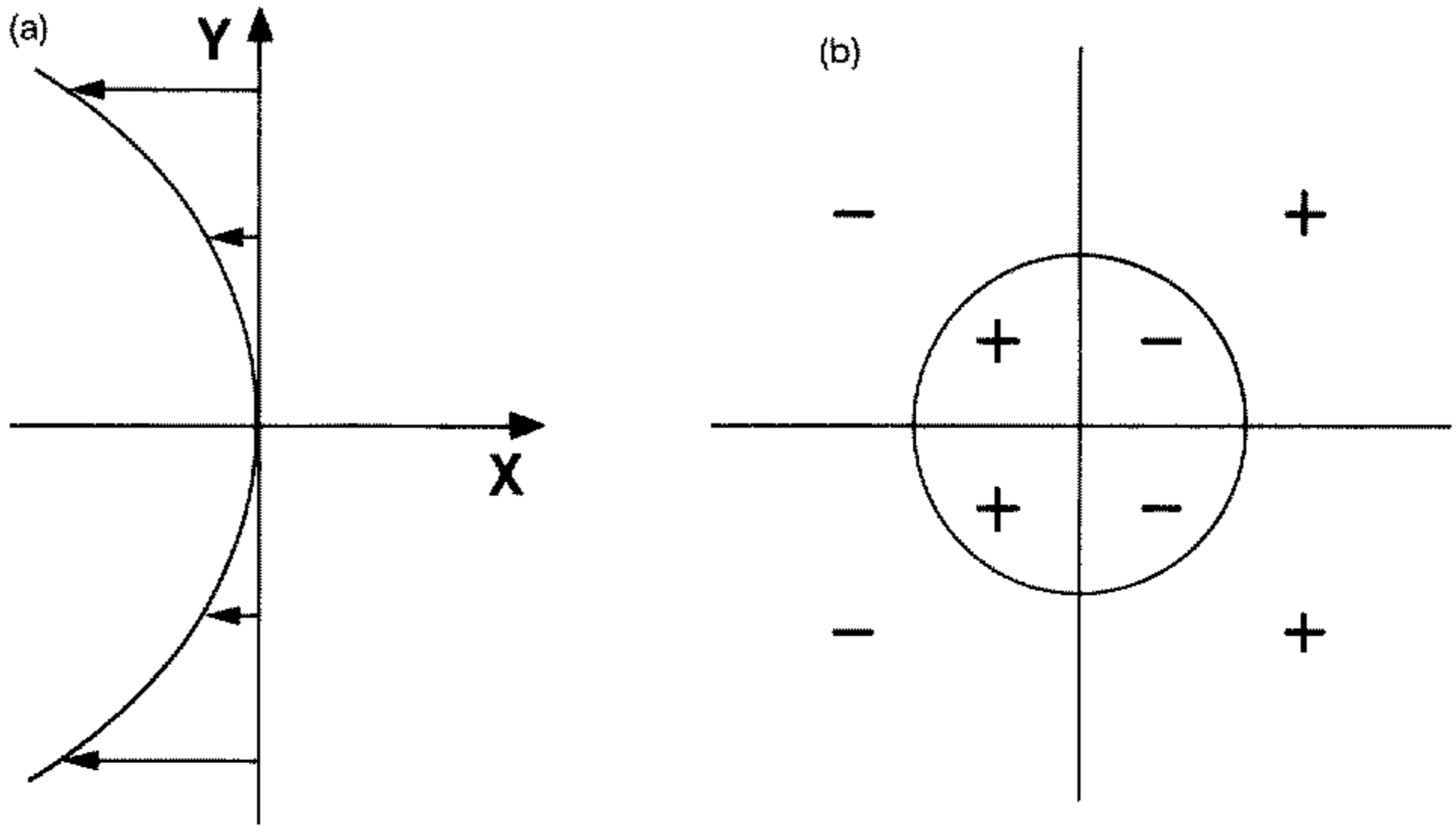

Figure 9. Schematic depiction of the wave-number-1 vorticity tendency arising from the term $-\overline{\mathbf{U}} \cdot \nabla\zeta = -\overline{U}\zeta_X$ in the case of linear basic shear $\overline{U} = \frac{1}{2}U''Y^2$; (a) shows the profile $\overline{U}(Y)$ and (b) shows the vorticity tendency $-\overline{U}\zeta_X$ in the eight regions defined in Fig. 5. The sign of ζ_X in these regions is shown in Fig. 5(a).

Figure 13 compares the analytically with the numerically calculated vorticity asymmetry at 24 hours for the case in which $\Gamma_{y0} = \beta_{st}$ and $\beta = 0$, designated here as SNB, and corresponding with the case 3B2 in US. The difference between these asymmetries when centred together are shown in Fig. 12(b). Again, the patterns show very good overall agreement, but there are small differences to the north-east and north-west of the vortex. It is clear, however, that the analytic theory captures the principal features of the numerical calculation.

A feature of all the fields in Figs. 6, 7, 11 and 13 is the large scale of the asymmetries, the extreme values of which are located on the order of 500 km from the vortex centre, similar to the zero-order asymmetry. This is a result of large particle displacements at these radii (see section 7). At inner radii the large angular shear of the vortex produces narrow spiral regions of vorticity of alternating sign. As discussed by Smith *et al.* (1990, p. 351), the integrated effect of these spirals makes a relatively small contribution to the stream function, and hence to the associated stream flow across the vortex centre. For this reason also, the inner core differences in the vorticity asymmetries evident in Figs. 8 and 12 are of little consequence in regard to vortex motion.

A summary of the various contributions to the vorticity asymmetry as detailed above is given in Table 1.

(c) *Stream-function asymmetries*

An analytic expression for the asymmetric stream function may be obtained as follows. Contributions to the asymmetric vorticity, $\hat{\xi}$, are associated with stream-function contributions, $\hat{\psi}$, satisfying $\nabla^2\hat{\psi} = \hat{\xi}$; in particular, vorticity contributions of the form $\hat{\xi} = \tilde{\xi}_n(r,t)\cos(n\theta + \alpha)$, $(n = 0, 1, 2, \ldots n)$, correspond with stream-function contributions of the same form: $\hat{\psi}_n(r,t)\cos(n\theta + \alpha)$, where α is a constant and

$$\psi_0 = \int_0^r \frac{dp}{p} \int_0^s s\tilde{\xi}_0(s,t)\, ds \tag{5.1a}$$

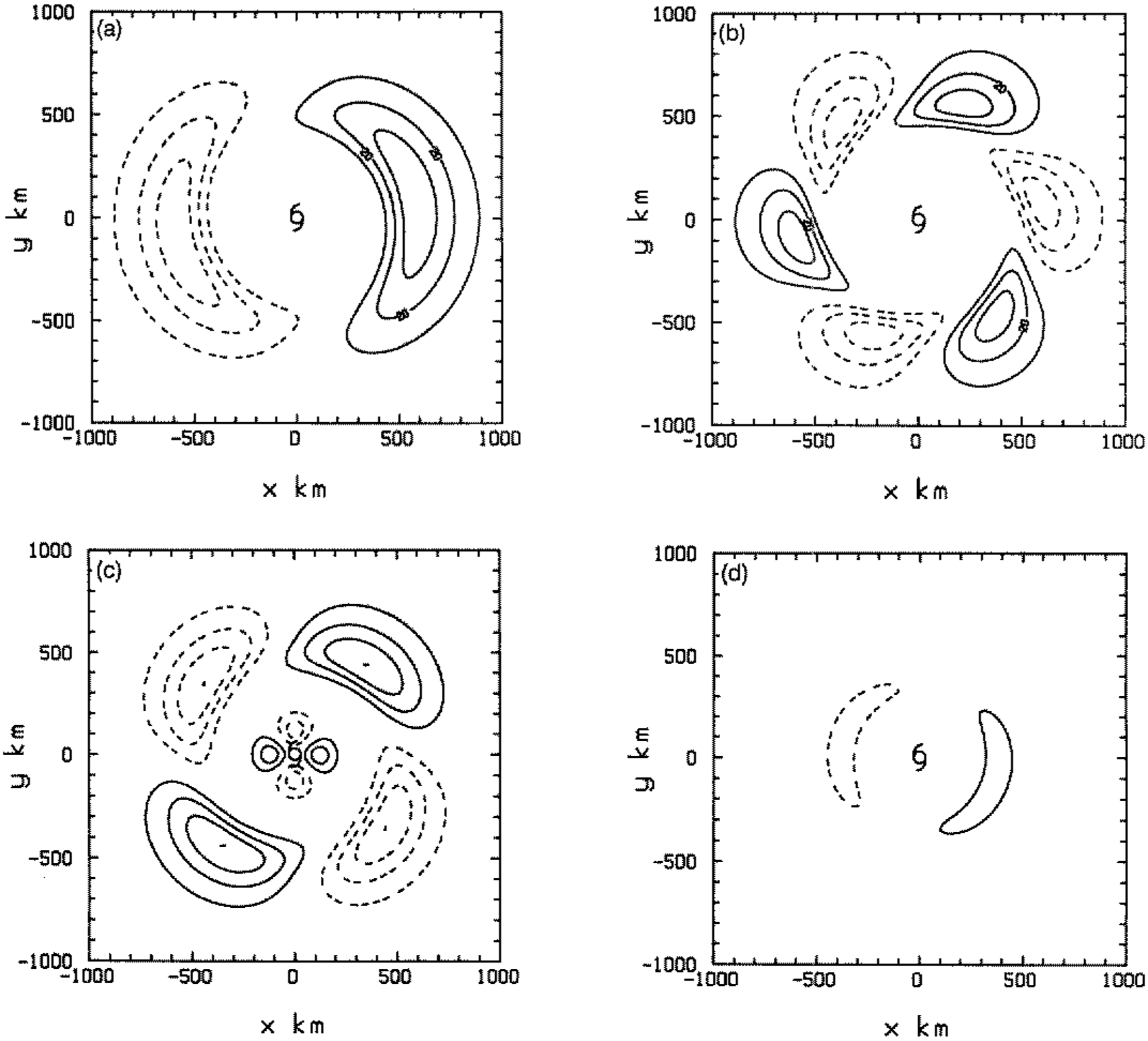

Figure 10. Contribution to the vorticity asymmetry Γ_{14} from (a) wave number 1, (b) wave number 3 and (c) wave number 2 for the linear shear case, SHB (see text for explanation) at 24 hours; (d) shows the wave-number-1 contribution to Γ_{51}. Contour interval is $1.0 \times 10^{-6}\,s^{-1}$ in (a) and (b) and $2.0 \times 10^{-7}\,s^{-1}$ in (c) and (d). Dashed lines indicate negative values. The vortex centre, marked by a cyclone symbol, is at the centre of each panel.

$$\psi_n = \frac{1}{2n}\left\{r^n \int_r^\infty p^{1-n}\bar{\xi}_n(p,t)\,dp - r^{-n}\int_0^r p^{1+n}\bar{\xi}_n(p,t)\,dp\right\}. \qquad (n \neq 0). \quad (5.1b)$$

Note that symmetric vorticity components correspond with $n = 0$, $\alpha = 0$ and terms involving $\sin n\theta$ with $\alpha = -\pi/2$. The integrals in Eq. (5.1) can be readily evaluated by quadrature from the expressions $\zeta_{ij}(r,t)$ etc. in sections 4(a)–4(e). Thereby the stream function corresponding with the total asymmetric vorticity $\Gamma_0 + \Gamma_1$, or any component thereof, can be easily calculated.

Figure 14 compares the asymmetric stream function calculated in this way with that from the corresponding numerical model simulation of US at 24 hours for the four cases discussed in sections 5(b)(i) and 5(b)(ii) above. To minimize the effects of boundary distortion arising from the finite domain in the numerical model, the model calculations were repeated using a 4000 km × 4000 km domain, twice the size of that employed by US, but comparisons are confined to a 2000 km × 2000 km domain. In broad terms, the

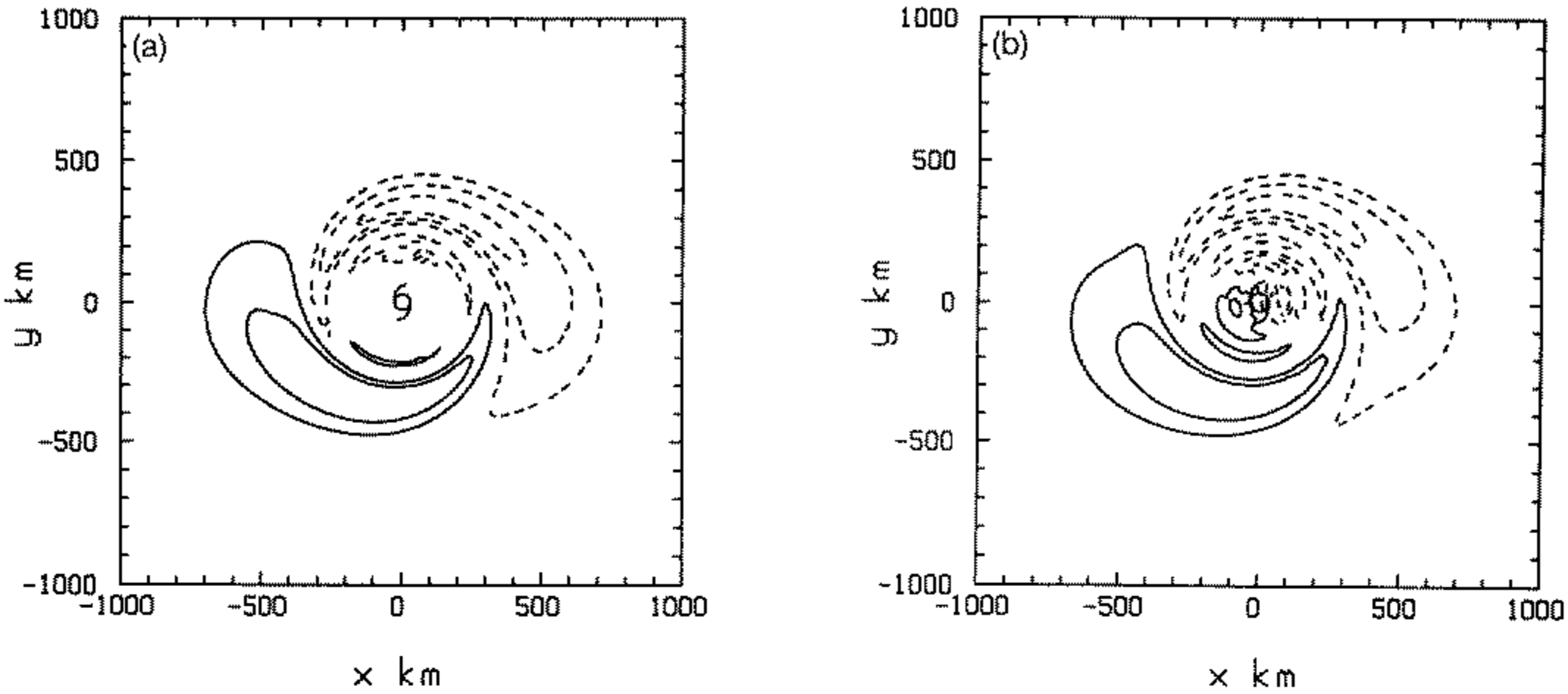

Figure 11. Total asymmetric vorticity field for the case of linear basic shear (SHB) (see text for explanation) at 24 hours. (a) Analytical calculation and (b), the corresponding numerical calculation (the case 3B1 of US). Contour interval is $5.0 \times 10^{-6}\,s^{-1}$. Dashed lines indicate negative values. The vortex centre, marked by a cyclone symbol, is at the centre of each panel.

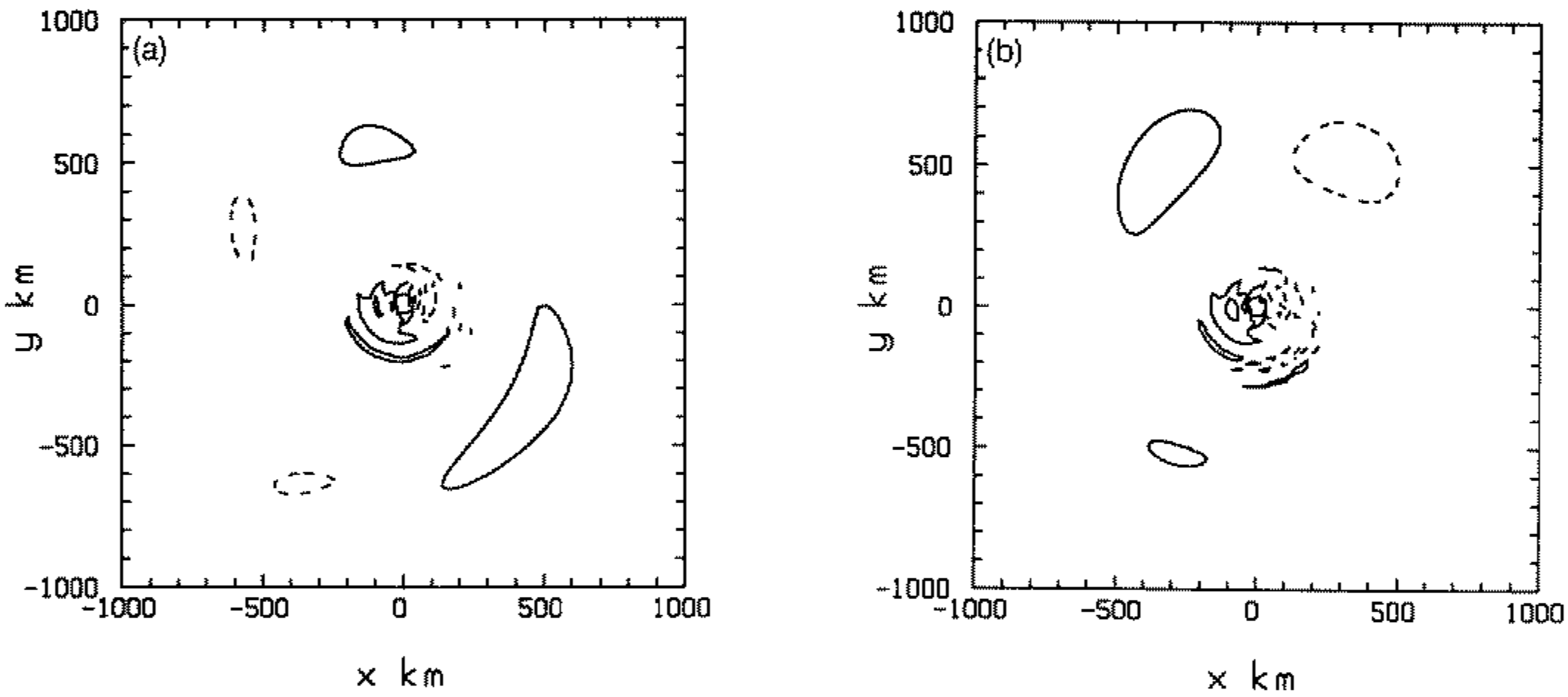

Figure 12. As for Fig. 8, but for the linear shear cases (a) SHB, (b) SNB. (See text for explanation.)

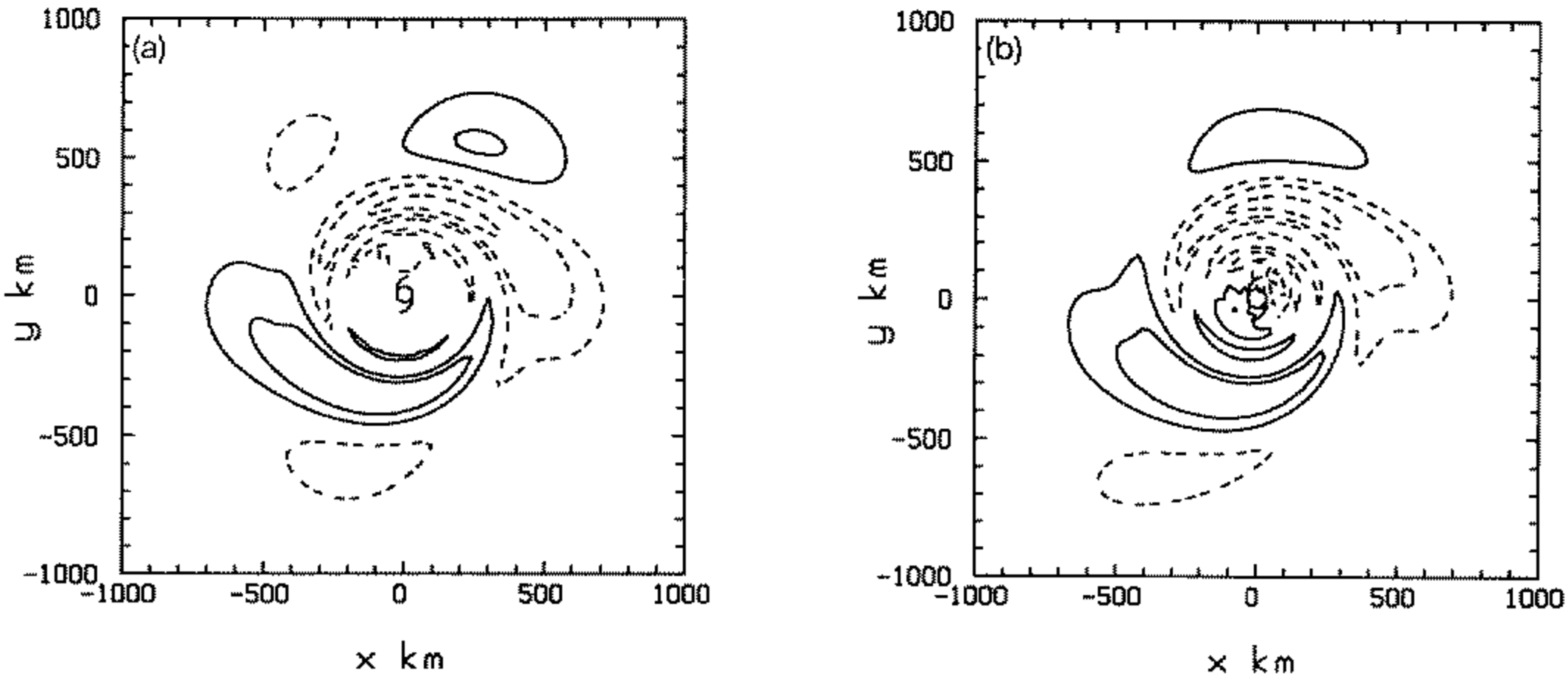

Figure 13. As for Fig. 11, but for the case SNB (the case 3B2 of US). (See text for explanation.)

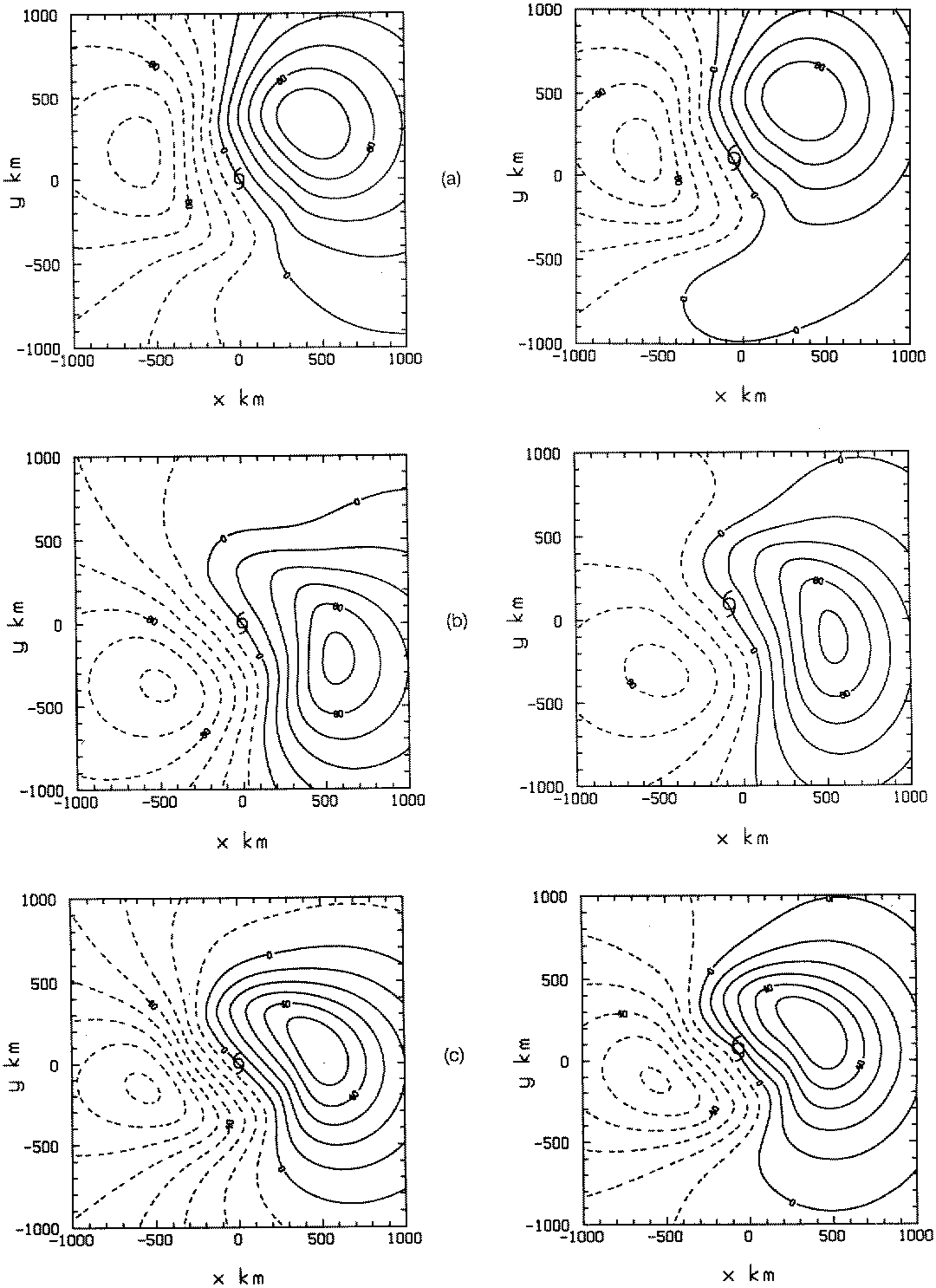

Figure 14. Total asymmetric stream-function fields at 24 hours for the uniform and linear shear calculations described in section 5: (a) case LP1, (b) case LN, (c) case SHB, and (d) case SNB. (See text for explanation.) Contour interval is $2.0 \times 10^5\,m^2\,s^{-1}$ in (a) and (b) and $1.0 \times 10^5\,m^2\,s^{-1}$ in (c) and (d). Left-side panels are for the analytical calculations. In each case the streamlines are shown for a *fixed* frame. In the numerical calculations the vortex centre (marked by a cyclone centre) is displaced from the origin, the initial vortex position. In the analytic calculations the vortex is at the centre of coordinates.

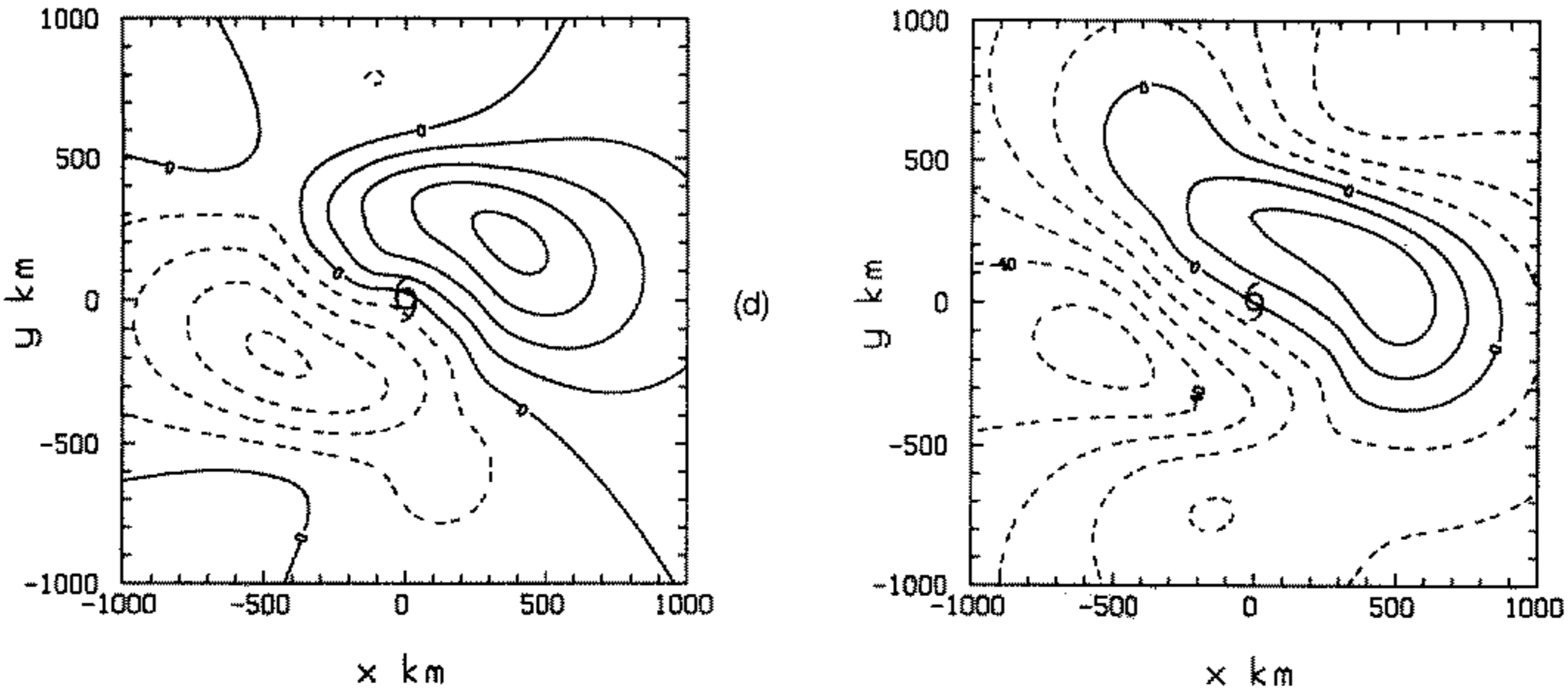

Figure 14. Continued.

correspondence of the fields is very good, a further indication that the analytic model captures the essential features of the numerical solution and presumably, therefore, of the dynamics of vortex motion.

However, there are some differences in detail; in particular, the maximum and minimum gyre strengths are not predicted accurately in most cases, and in case SNB the far field structure is not well represented by the theory. These differences are presumably a reflection of the approximations made in deriving the theory which, *inter alia*, suppress planetary-wave propagation at lowest order. This omission would be likely to show up in the comparisons at large scale. The differences may be due also in part to the fact that the numerical calculation assumes channel boundary conditions at a finite distance from the vortex whereas the analytic solution is for an infinite domain.

TABLE 1. SUMMARY OF THE TERMS CONTRIBUTING TO THE VORTICITY ASYMMETRY Γ_a AND THEIR INTERPRETATION

Contribution to Γ_a	Vorticity term	Wave-number contributions 0	1	2	3	4	Interpretation
Γ_0	$-\mathbf{u}\cdot\nabla(\bar{\Gamma}+f)$		●				Advection of basic-state absolute vorticity by the vortex
Γ_{11}	$-\mathbf{U}_0\cdot\nabla\zeta$		●				Advection of vortex vorticity by the vortex asymmetry
Γ_{12}	$-\mathbf{U}_0\cdot\nabla(\bar{\Gamma}+f)$		●		●		Advection of basic-state absolute vorticity by the vortex asymmetry
Γ_{13}	$-\mathbf{U}_0\cdot\nabla\Gamma_0$		●		●		Self-advection of vortex asymmetry
Γ_{14}	$-\bar{\mathbf{U}}\cdot\nabla\zeta$	$\bar{\Gamma}_{0y}=0$			●		Advection of vortex vorticity
		$\bar{\Gamma}_0=0$		●		●	by the basic flow
Γ_{15}	$-\bar{\mathbf{U}}\cdot\nabla\Gamma_0$	$\bar{\Gamma}_{0y}=0$		●		●	Advection of vortex asymmetry
		$\bar{\Gamma}_0=0$	●	●	●	●	by the basic flow

Column 2 shows the term contributing to the Lagrangian vorticity tendency, $\partial\Gamma_a/\partial t+\mathbf{u}\cdot\nabla\Gamma_a$. Column 3 shows the azimuthal wave-number contribution of each term. Wave number 0 means an axisymmetric contribution. In the absence of shear the principal contribution to the asymmetry is from Γ_0 and Γ_{11}. The relative contributions of Γ_{14} and Γ_{15} depend on the strength and nature of the shear.

6. VORTEX TRACK

Equation (3.9) provides an analytic expression for the zero-order vortex translation velocity in terms of integrals of the zero-order vorticity components, ζ_1 and ζ_2, in Eq. (3.3) (cf. Eq. (3.10)). The vortex track $x_0(t) = \{x_0(t), y_0(t)\}$ may be obtained for the zero-order solution simply by integrating the equation

$$\frac{d\mathbf{x}_0}{dt} = \mathbf{c}(t) \tag{6.1}$$

with $\mathbf{c}(t)$ given by Eq. (3.9). It follows that

$$\begin{bmatrix} x_0(t) \\ y_0(t) \end{bmatrix} = \begin{bmatrix} F_2(t) & F_1(t) \\ -F_1(t) & F_2(t) \end{bmatrix} \begin{bmatrix} \cos\theta_* \\ \sin\theta_* \end{bmatrix} \tag{6.2}$$

where

$$F_n(t) = \tfrac{1}{2}r \int_0^\infty \left\{ \int_0^t \zeta_n(p, t)\, dt \right\} dp, \; (n = 1, 2). \tag{6.3}$$

The track correction, $\Delta\mathbf{x}_1$, associated with first-order vorticity correction, Γ_1, may be obtained in a similar way. Symmetry considerations imply that only wave-number-1 components of Γ_1 contribute to the vortex motion, i.e. to a nonzero asymmetric flow across the vortex centre. Therefore, for a zonal shear flow in which $\theta_* = 0$ (see Eqs. (2.10) and (3.5b))

$$\Delta\mathbf{x}_1 = (\Delta F_2 \cos\theta, -\Delta F_1 \sin\theta) \tag{6.4}$$

where

$$\Delta F_n = \tfrac{1}{2}r \int_0^\infty \left\{ \int_0^t (\zeta_{1\nu} + \zeta_{41\nu} + \zeta_{51\nu})\, dt \right\} dp \tag{6.5}$$

and the suffix ν equals c for $n = 1$ and s for $n = 2$. Using the expressions for the vorticity contributions given in the appendices, the inner (i.e. time) integrals may be performed analytically and the outer integrals are again easily evaluated using quadrature.

In the case of zonal shear there is an additional component of the vortex motion resulting from the basic flow across the vortex centre; this is represented by the first term on the right-hand side of Eq. (2.8). The associated displacement $\Delta\mathbf{x}_2$, which must be added to $\mathbf{x}_0 + \Delta\mathbf{x}_1$ to calculate the vortex track, can be obtained as follows. Suppose that during the time interval Δt, the vortex undergoes a meridional displacement, Δy, from y_1 to y_2 with mean speed $\bar{c}_2 = \Delta y/\Delta t$. During this time the vortex will undergo a zonal displacement

$$\Delta x_2 = \int_0^{\Delta t} \overline{U}(y)\, dt \doteq \frac{1}{\bar{c}_2} \int_{y_1}^{y_2} \overline{U}(y)\, dy. \tag{6.6}$$

In our case this becomes

$$\Delta x_2 = \Delta t\{\overline{U}_0 + \overline{U}_{y0}\bar{y} + \tfrac{1}{2}\overline{U}_{0yy}(\bar{y}^2 + \tfrac{1}{12}\Delta y^2)\} \tag{6.7}$$

where $\bar{y} = (y_1 + y_2)/2$ and $\Delta y = y_2 - y_1$.

The analytically calculated vortex tracks for three uniform shear cases LP1, LP2 and LN are shown in Fig. 15(a) where they are compared with the corresponding numerically predicted tracks. The three cases are identical with the cases 3A1 – 3A3 of US, but the numerically predicted tracks shown in Fig. 15(a) were for a larger domain

(4000 km × 4000 km) than in US. The numerical calculations were repeated here because it is known that there is some dependence of the track on domain size for smaller domain sizes, the deviations increasing with time (see for example Fiorino 1987). The analytic calculation highlights the two effects of uniform shear on the vortex track compared with the case of zero basic flow: a zonal displacement caused by advection with the basic flow as the vortex tracks across the shear, and a predominantly meridional displacement associated with the wave-number-1 asymmetry in Γ_{15}. This asymmetry, exemplified by the vorticity distribution shown in Fig. 6(b) for the case LP1, causes an additional poleward displacement for positive shear and an equatorward displacement for negative shear. Note that these track differences are independent of the basic-state absolute-vorticity gradient which is the same (i.e. β_{st} for each case).

The tracks for the two linear shear cases SHB and SNB, corresponding with the cases 3B1 and 3B2 of US, are shown in Fig. 15(b) together with the corresponding numerical calculations of US for the larger domain. Differences in the tracks compared with the case of zero basic flow are again attributable to zonal displacement as the vortex moves across a varying basic flow and to a predominantly meridional displacement associated with the wave-number-1 asymmetry. The asymmetry is dominated by the contribution from Γ_{141}, shown in Fig. 10(a) for the case SHB, and gives an equatorward displacement for negative $\overline{U}_{yy0}$, the case illustrated. The magnitude of the displacement is proportional to the magnitude of $\overline{U}_{yy0}$. There is a small meridional contribution to the track from the wave-number-1 asymmetry in Γ_{151} when $\overline{U}_{yy0}$ is nonzero. However, this is negligible in the case SHB, the contribution at 48 hours being less than 1%.

As in the case of zero basic flow (SU, Fig. 5), the analytically and numerically calculated tracks agree remarkably well in all cases, at least until 24 hours. At later times the analytic theory over-estimates the vortex speed in comparison with the numerical calculation, except in the case of zero beta, but in all cases the track directions agree closely until 48 hours. The smaller speed in the numerical calculations at later times may be due in part to the increasing influence of the domain boundaries (the analytic theory assumes an infinite domain), but is more likely to be a reflection of the progressive breakdown of the analytic theory at large times.

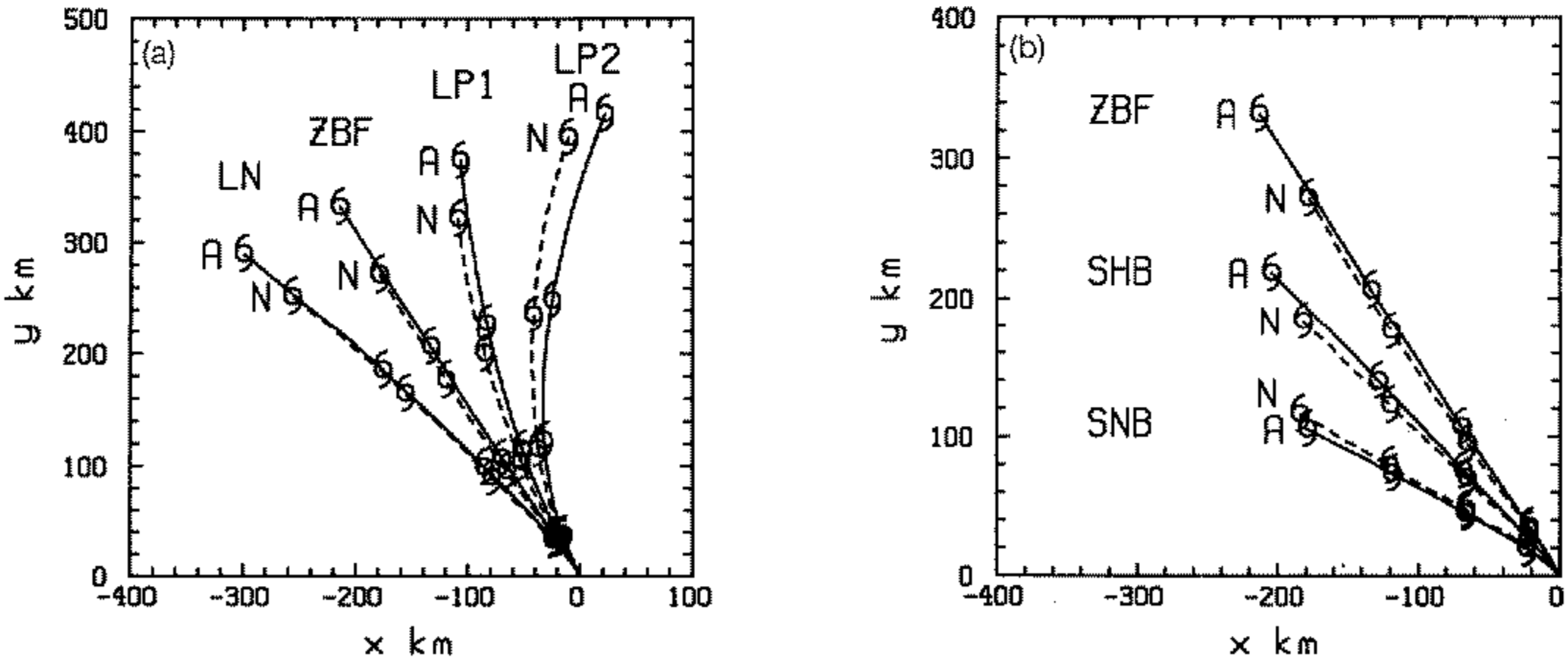

Figure 15. Analytically calculated vortex track (denoted by A) compared with the corresponding numerical solution (denoted by N): (a) uniform shear flow cases and (b) linear shear flow cases. Each panel includes the analytically and numerically calculated track for the case of zero basic flow (denoted ZBF). Cyclone symbols mark the vortex position at 12-hour intervals. (See text for explanation of other letters.)

Note that the excellent comparison in the tracks to 48 hours in the case SNB is despite the relatively poor comparison of the stream-function fields at large distances in this case (see Fig. 14(d)). Evidently, the theory predicts the wave-number-1 asymmetry adequately, since the track depends only on this component.

7. Limitations of the theory

The breakdown of the theory is discussed briefly by SU at the end of section 3. In essence, the linearization assumption that air-parcel trajectories are approximately circular about the vortex centre is no longer valid at larger radii where tangential wind speeds are comparable with or less than the speed of vortex motion and/or that of basic flow. For a stationary symmetric vortex, the maximum meridional displacement of an air parcel at radius r would be $2r$, so that the maximum asymmetric vorticity perturbation associated with the beta effect would be $-2\beta r$, i.e. this increases with r. Given sufficient time, parcels at large radii from the vortex have the potential to produce larger vorticity perturbations than those at inner radii, and there would be no limit to the radial scale of the asymmetric gyres. This is confirmed by calculations of zero-order asymmetry $\Gamma_0(r, \theta, t)$ at large times and is implicit in the theory of gyre structure given in section 4 of Smith *et al.* (1990). An important consequence is that the zero-order vortex speed given by Eq. (3.9) increases indefinitely, although the rate of increase is relatively slow after an initial growth period (Fig. 16). Interestingly, the zero-order track remains remarkably unidirectional during this time (see SU, Fig. 5).

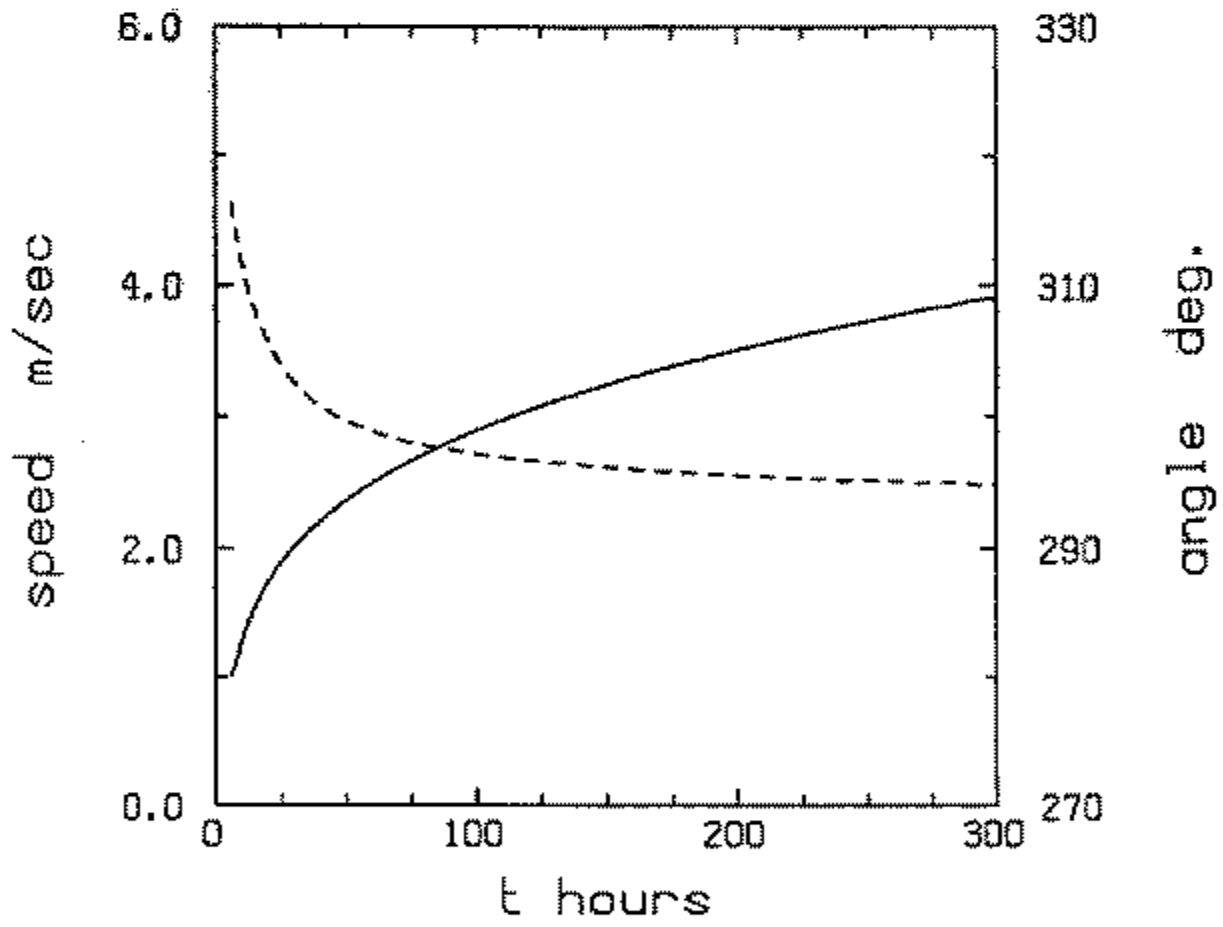

Figure 16. Variation with time of the zero-order vortex speed (solid line) and direction (dashed line) to 300 hours in the case of zero basic flow.

In practice, of course, the vortex translates, and if its tangential velocity decreases monotonically to zero with radius r, there will be some radius, r_*, beyond which the relative motion on one side of it (to the east for a cyclonic vortex translating polewards) will be anticyclonic (SU, Fig. 12). If the anticyclonic symmetric circulation change exemplified in Fig. 4 were to be regarded as part of the vortex circulation this would further reduce r_*. If shear is present, it will generally dominate the vortex circulation at large radii, again invalidating the zero-order asymmetry calculation in this region. We hypothesize that the omission of these effects is a primary reason for the difference between the analytically and numerically calculated tracks at larger times and are

currently investigating this aspect further. In particular, it remains to be shown whether or not the excellent agreement in the tracks out to 48 hours for the case SNB is fortuitous. We may presume that the neglect of nonlinear interaction between the various wave-number components of the vortex asymmetry is also a limitation in the accuracy of the analytic solutions at later times.

8. Discussion

The availability of an analytic theory of vortex motion not only provides a deeper insight into the basic processes of vortex motion, but also enables the vortex-induced asymmetries to be calculated for a specified environmental flow at a specified time. This offers the possibility of designing more appropriate 'bogus' vortices for the initialization of tropical-cyclone forecast models, a problem that was touched on in SU. It should be possible, for example, to design an asymmetric bogus vortex that will have an initial speed and direction that matches the observed speed and direction of the cyclone in question. For this purpose it may be sufficient to use only the wave-number-1 contributions to the asymmetry as detailed in section 4 and the appendices. Investigations relating to such applications of the theory are continuing.

Consideration of the initialization problem raises also the question of the existence of a steady-state solution for motion. Although the present analytic theory breaks down after a certain time, the processes contributing to the evolution of the vorticity field that have been identified must continue to operate; only the feedbacks are missing in the theory (i.e. the first-order symmetric flow correction will contribute to advection of absolute vorticity about the vortex centre, and the velocity correction to the vortex speed from the first-order wave-number-1 asymmetry will affect the relative flow around the vortex). Notwithstanding the fact that, in the absence of a basic flow, vortices tend to achieve a quasi-steady speed and direction (Chan and Williams 1987, see Fig. 6; Fiorino and Elsberry 1989a, see Fig. 11), it appears that their vorticity structure continues to evolve, both in the core region owing predominantly to the large angular shear of the tangential wind component (Shapiro and Ooyama 1990; Smith *et al.* 1990) and at larger radii owing to the excitation of planetary waves (Chan and Williams 1987). This may be expected to be more so for the case in the presence of horizontal shear because, unless the shear is uniform, vortices will move into regions of changing effective β (i.e. B_*), whereupon the asymmetries must continue to evolve in structure. Under these circumstances it would appear that a true steady state is unlikely to exist. Even uniform shear will have a sustained effect on the evolution of the vorticity asymmetry, stretching it out into longer and narrower filaments much as the angular shear of the tangential wind acts in the vortex-core region. It is not obvious what processes could balance these effects in the inviscid model investigated here.

The foregoing theory supposes that the particular vortex profile chosen is not unstable to small amplitude disturbances of some form. That this would not be the case is suggested by a stability analysis of circular vortices by Gent and McWilliams (1986) (see also SU, section 3), and has been confirmed by detailed calculations of Weber (1991).

The calculations presented herein are for horizontal shears that are relatively weak, but which are typical, nonetheless, of a tropical-cyclone environment. Large shear on the scale of the vortex may be expected to produce a large distortion of the vortex, thereby invalidating the linearization about the basic vortex inherent in the present method. Indeed, it may even destroy the vortex. An example was presented by Smith *et al.* (1990, see Fig. 14 and the related discussion therein) in the context of a multiple

vortex interaction. In this case, a weaker vortex was subjected to the angular shear of a stronger one. After a certain time, the vorticity field of the weaker vortex was sheared out into a long thin filament of vorticity along an arc of the larger vortex.

9. Conclusions

The effects of a basic horizontal shear flow on the motion of a barotropic vortex on a beta plane have been identified and quantified through the development of an approximate analytic theory. The effects are characterized by the contribution of the shear-related terms in the (environmental) vorticity equation to the evolution and structure of the wave-number-1 component of the vorticity asymmetry. The vorticity asymmetry has an associated stream-function pattern consisting of a pair of counter-rotating gyres analogous to the beta gyres in the case of zero basic flow.

The effects of shear have been illustrated for the case of a zonal flow with a linear or quadratic variation in wind speed. A linear wind profile, i.e. uniform shear, induces a first-order wave-number-1 vorticity correction by differentially advecting the existing wave-number-1 asymmetry, but it does not affect the absolute-vorticity gradient and therefore the zero-order asymmetry. In contrast, a quadratic wind profile makes a wave-number-1 vorticity correction by differentially advecting the *vortex* vorticity; it contributes also to the absolute-vorticity gradient and thereby to the magnitude of the zero-order asymmetry. Both these effects influence the vortex track, but not to the same degree. Accordingly, vortex motion cannot be characterized by the basic-state absolute-vorticity gradient alone—the proportionate contribution of the shear to the absolute-vorticity gradient is important also. Finally, the displacement of the vortex centre from its initial position leads also to a small wave-number-1 contribution to the asymmetry, and hence to vortex motion.

The asymmetric vorticity and stream-function patterns predicted by the analytic theory agree well with those computed by solving the problem numerically, as do the vortex tracks for a period up to 48 hours. Ultimately, the analytic theory breaks down for reasons that appear, *inter alia*, to be linked with the breakdown of the zero-order solution. The emergence of significant nonlinear interactions between the various wave-number components of the vortex asymmetry may contribute also to the breakdown, an effect that is expected to increase in importance with the magnitude of the shear.

Acknowledgements

I would like to thank my colleague Wolfgang Ulrich who kindly reran the numerical calculations of our earlier paper on a larger domain so that they could be used here for comparison with the present theory. I am grateful also to Harry Weber who patiently helped me to check the algebraic calculations and computer code. Thanks go also to Karin Brückner who capably prepared the manuscript and to Herr H. Wendt who drew some of the figures.

This work was supported by the US Office of Naval Research through grant No. N00014–90–J–1487.

APPENDIX 1

Calculation of ζ_{2v}, ζ_{3v}

Differentiating Eq. (3.8) with respect to r gives

$$\frac{\partial \psi_n}{\partial r} = \tfrac{1}{2}\int_0^r \left(1 + \frac{p^2}{r^2}\right) \zeta_n(p, t)\, dp$$

whereupon, using Eq. (3.8) itself together with Eq. (3.4), Eqs. (4.8) give

$$A_2(r, t) = \tfrac{1}{2}B_*^2 \int_0^r p \sin(\Omega_p t)\, dp$$

$$B_2(r, t) = \tfrac{1}{2}B_*^2 r^{-2} \int_0^r p^3 \sin(\Omega_p t)\, dp$$

$$C_2(r, t) = \tfrac{1}{2}B_*^2 r^{-2} \int_0^r p^3 \{1 - \cos(\Omega_p t)\}\, dp.$$

Here and later we denote $\Omega(\nu)$ by Ω_ν. Then the second two terms on the right-hand side of Eq. (4.7) may be written

$$\tfrac{1}{2}B_*^2 r^{-2} \int_0^r p^2 \{\sin 2\overline{\theta} - \sin(2\overline{\theta} - \Omega_p t)\}\, dt.$$

The integration of this with respect to time following a hypothetical fluid parcel from its initial position (r, θ_0) along the circle to (r, θ) is accomplished by setting $\theta = \theta_0 + \Omega_r t$ before integrating, while A_2 can be integrated directly. Thereby, Eq. (4.9) integrates to give Eq. (4.10), where

$$\zeta_{20}(r, t) = \tfrac{1}{2}B_*^2 \int_0^r p \left\{\frac{1 - \cos(\Omega_p t)}{\Omega_p}\right\} dp$$

$$\zeta_{2c}(r, t) = \tfrac{1}{2}B_*^2 r^{-2} \int_0^r p^3 \left\{\frac{\cos(2\Omega_r t) - 1}{2\Omega_r} - \frac{\cos(2\Omega_r t) - \cos(\Omega_p t)}{2\Omega_r - \Omega_p}\right\} dp$$

$$\zeta_{2s}(r, t) = \tfrac{1}{2}B_*^2 r^{-2} \int_0^r p^3 \left\{\frac{\sin(2\Omega_r t)}{2\Omega_r} - \frac{\sin(2\Omega_r t) - \sin(\Omega_p t)}{2\Omega_r - \Omega_p}\right\} dp.$$

It is interesting to note that $\zeta_{20}(\infty, t) = B_* y_c$, y_c being the meridional displacement of the vortex as predicted by the zero-order theory. Accordingly, it represents the change in basic state absolute vorticity of every vortex particle due to the meridional displacement of the vortex. This term is exactly cancelled by the sum of $\overline{\Gamma}_f$, defined in section 2, and the additional term $\mathbf{x}_c \cdot \nabla_{\mathbf{x}} \overline{\Gamma}_0 = y_c \overline{\Gamma}_{0y}$ on the right of Eq. (2.9) which was earlier neglected. Thus, in calculating the change of relative vorticity and, in particular, the change in the symmetric wind component associated with the vortex motion, the value $\zeta_{20}(\infty, t)$ must be subtracted from the vorticity correction $\zeta_{20}(r, t)$. This was done in calculating the vortex asymmetries throughout this paper.

The expression for Γ_{13} is obtained in a similar manner. For example, in Eq. (4.11), the expression for $A_3(r, t)$ is

$$\tfrac{1}{2}\left(\frac{\partial \zeta_1}{\partial r}\frac{\Psi_2}{r} - \frac{\partial \zeta_2}{\partial r}\frac{\Psi_1}{r} + \frac{\partial \Psi_2}{\partial r}\frac{\zeta_1}{r} - \frac{\partial \Psi_1}{\partial r}\frac{\zeta_2}{t}\right)$$

with similar ones for B_3 and C_3. These can be reduced to integrals with respect to p of functions of r, p and t; for example

$$A_3 = \tfrac{1}{2}B_*^2 \left[\int_0^r p\{\sin(\Omega_r t) - \sin(\Omega_p t) - \sin(\Omega_r - \Omega_p)t\}\, dp + \right.$$

$$\left. + \tfrac{1}{2}\mu\Omega_r \int_0^r p\left(1 - \frac{p^2}{r^2}\right)\{\cos(\Omega_r t) - \cos(\langle\Omega_r - \Omega_p\rangle t)\}\, dp \right].$$

Similar expressions are obtained for B_3 and C_3. The latter must be combined with the $\cos 2\theta$ and $\sin 2\theta$, as in the calculation of Γ_{12}. Again, since A_3 is independent of θ, it can be integrated directly with respect to time, while, in the expression for $B_3 \cos 2\theta + C_3 \sin 2\theta$ it is necessary to substitute $\theta = \theta_0 + \Omega_r t$ before integration. After several steps of tedious, but straightforward algebra, we obtain the following expressions for $\zeta_{3\nu}$ in Eq. (4.13):

$$\zeta_{30}(r,t) = -\zeta_{20}(r,t) + \tfrac{1}{2}B_*^2 \left[\int_0^r p \left\{ \frac{1 - \cos\Omega_r t}{\Omega_r} - \frac{1 - \cos(\Omega_r - \Omega_p)t}{\Omega_r - \Omega_p} \right\} dp + \right.$$

$$+ \tfrac{1}{2}r\Omega' \int_0^r p\left(1 - \frac{p^2}{r^2}\right) \left\{ \frac{\cos\Omega_r t - 1 + \Omega_r t \sin\Omega_r t}{\Omega_r^2} + \right.$$

$$\left. \left. + \frac{1 - \cos(\Omega_r - \Omega_p)t - (\Omega_r - \Omega_p)t\sin(\Omega_r - \Omega_p)t}{(\Omega_r - \Omega_p)^2} \right\} dp \right]$$

$$\zeta_{3c}(r,t) = -\zeta_{2c}(r,t) + \tfrac{1}{2}B_*^2 \left[\int_0^r \frac{p^3}{r^2} \left\{ \frac{\cos 2\Omega_r t - \cos\Omega_r t}{\Omega_r} - \frac{\cos 2\Omega_r t - \cos(\Omega_r + \Omega_p)t}{\Omega_r - \Omega_p} \right\} dp - \right.$$

$$- \tfrac{1}{2}r\Omega' \int_0^r p\left(1 - \frac{p^2}{r^2}\right) \left\{ \frac{\cos(\Omega_r + \Omega_p)t - \cos 2\Omega_r t}{(\Omega_r - \Omega_p)^2} - \frac{(\Omega_r - \Omega_p)t\sin(\Omega_r + \Omega_p)t}{(\Omega_r - \Omega_p)^2} - \right.$$

$$\left. \left. - \frac{\cos\Omega_r t - \cos 2\Omega_r t - \Omega_r t \sin\Omega_r t}{\Omega_r^2} \right\} dp \right]$$

$$\zeta_{3s}(r,t) = -\zeta_{2s}(r,t) + \tfrac{1}{2}B_*^2 \left[\int_0^r \frac{p^3}{r^2} \left\{ \frac{\sin 2\Omega_r t - \sin\Omega_r t}{\Omega_r} - \frac{\sin 2\Omega_r t - \sin(\Omega_r + \Omega_p)t}{\Omega_r - \Omega_p} \right\} dp - \right.$$

$$- \tfrac{1}{2}r\Omega' \int_0^r p\left(1 - \frac{p^2}{r^2}\right) \left\{ \frac{\sin(\Omega_r + \Omega_p)t - \sin 2\Omega_r t}{(\Omega_r - \Omega_p)^2} + \frac{(\Omega_r - \Omega_p)t\cos(\Omega_r + \Omega_p)t}{(\Omega_r - \Omega_p)^2} - \right.$$

$$\left. \left. - \frac{\sin\Omega_r t - \sin 2\Omega_r t + \Omega_r t \cos\Omega_r t}{\Omega_r^2} \right\} dp \right]$$

where Ω' denotes $d\Omega/dr$.

APPENDIX 2

Calculation of $\xi_{44\nu}$

The first three contributions Γ_{14i} to Γ_{14} satisfy an equation of the form

$$\frac{d\Gamma_*}{dt} = G\cos n\theta + H\sin n\theta$$

where G and H are functions only of r, and d/dt means differentiation following the hypothetical air parcel referred to in Appendix 1. Accordingly, the equation may be integrated in the form

$$\Gamma_* = \int_0^t \{G \cos n(\theta_0 + \Omega_r t') + H \sin n(\theta_0 + \Omega_r t')\}\, dt'$$

to give

$$\Gamma_* = \{GS(r, n) - HC(r, n)\} \cos n\theta + \{GC(r, n) + HS(r, n)\} \sin n\theta,$$

where $C(r, n) = \{1 - \cos(n\Omega_r t)\}/(n\Omega_r)$ and $S(r, n) = \sin(n\Omega_r t)/(n\Omega_r)$.

For a zonal shear flow, the fourth term on the right-hand side of Eq. (4.14) is identically zero and the last term reduces to

$$-\tfrac{1}{2} r \frac{d\zeta}{dr} y_c \overline{U}_{yy0} \sin 2\theta$$

where

$$y_c = \tfrac{1}{2} B \int_0^\infty p \left(\frac{1 - \cos \Omega_p t}{\Omega_p} \right) dp. \tag{A2.1}$$

Therefore Γ_{144} satisfies

$$\frac{d\Gamma_{144}}{dt} = -\tfrac{1}{4} r \frac{d\zeta}{dr} \overline{U}_{yy0} B \int_0^\infty p \frac{(1 - \cos \Omega_p t)}{\Omega_p} \sin(2\theta_0 + 2\Omega_r t)\, dp.$$

This may be integrated with respect to time to give Eq. (4.16d) where, after a little algebra,

$$\zeta_{44c}(r, t) = \tfrac{1}{8} r \frac{d\zeta}{dr} \overline{U}_{yy0} B \int_0^\infty \frac{p}{\Omega_p} \left(\frac{1 - \cos 2\Omega_r t}{\Omega_r} + \frac{\cos 2\Omega_r t - \cos \Omega_p t}{2\Omega_r + \Omega_p} + \right.$$
$$\left. + \frac{\cos 2\Omega_r t - \cos \Omega_p t}{2\Omega_r - \Omega_p} \right) dp$$

and

$$\zeta_{44s}(r, t) = -\tfrac{1}{8} r \frac{d\zeta}{dr} \overline{U}_{yy0} B \int_0^\infty \frac{p}{\Omega_p} \left(\frac{\sin 2\Omega_r t}{\Omega_r} - \frac{\sin 2\Omega_r t + \sin \Omega_p t}{2\Omega_r + \Omega_p} - \right.$$
$$\left. - \frac{\sin 2\Omega_r t - \sin \Omega_p t}{2\Omega_r - \Omega_p} \right) dp..$$

APPENDIX 3

Calculation of ζ_{5nv}

For a zonal shear flow $\overline{\theta} = \theta$ and in Eq. (4.17) $\partial\Gamma_0/\partial X = \cos\theta\, \partial\Gamma_0/\partial r + (\sin\theta/r)\, \partial\Gamma_0/\partial\theta$, whereupon

$$-\overline{\overline{\mathbf{U}}} \cdot \nabla\Gamma_0 = (\overline{\overline{\Gamma}}_0 r \sin\theta + \tfrac{1}{2}\overline{\overline{\Gamma}}_{y0} r^2 \sin^2\theta + \overline{\overline{\Gamma}}_{y0} y_c r \sin\theta) \times$$
$$\times \{\cos\theta(\zeta_{1r} \cos\theta + \zeta_{2r} \sin\theta) - (\sin\theta/r)(\zeta_2 \cos\theta - \zeta_1 \sin\theta)\} \tag{A3.1}$$

where subscript r denotes the partial derivative $\partial/\partial r$. The second bracket on the right-hand side of this expression can be written

$$\tfrac{1}{2}\{\zeta_{1r} + \zeta_1/r + (\zeta_{1r} - \zeta_1/r)\cos 2\theta + (\zeta_{2r} - \zeta_2/r)\sin 2\theta\}$$

and, using Eq. (3.4) with $B_* = B$,

$$(\zeta_{1r} - \zeta_1/r, \zeta_{2r} - \zeta_2) = -Br\Omega' t(\cos \Omega t, \sin \Omega t)$$

and

$$\zeta_{1r} + 3\zeta_1/r = -Br\Omega' t \cos \Omega t - 4B \sin \Omega t.$$

Then the term in Eq. (A3.1) defines

$$\frac{d\Gamma_{151}}{dt} = -\tfrac{1}{2}\bar{\Gamma}_0 Br[\cos(\theta - \Omega t) - \cos(\theta + \Omega t) + 2\mu\Omega t\{\sin(\theta + \Omega t) + \sin(3\theta - \Omega t)\}]$$

where $\mu = \frac{1}{4}r\Omega'/\Omega$ and d/dt has the same meaning as in Appendix 2. This equation is readily solved by setting $\theta = \theta_0 + \Omega t$ and integrating with respect to t, treating θ_0 as a constant. After integration, θ_0 can be replaced by $\theta - \Omega(r)t$, giving an expression for Γ_{151} of the form

$$\Gamma_{151} = \zeta_{51c}\cos\theta + \zeta_{51s}\sin\theta + \zeta_{51c3}\cos 3\theta + \zeta_{51s3}\sin 3\theta$$

where

$$(\zeta_{51c}, \zeta_{51s}) = -\tfrac{1}{2}\bar{\Gamma}_0 Btr\left\{(1-\mu)\left(\cos\Omega t - \frac{\sin\Omega t}{\Omega t}\right), (1+\mu)\sin\Omega t\right\}$$

and

$$(\zeta_{51c3}, \zeta_{51s3}) = \tfrac{1}{2}\bar{\Gamma}_0 Btr\mu\left(\cos\Omega t + \frac{\sin\Omega t - \sin 3\Omega t}{2\Omega t}, \sin\Omega t + \frac{\cos 3\Omega t - \cos\Omega t}{2\Omega t}\right).$$

Expressions for ζ_{520}, ζ_{52c}, ζ_{52s}, ζ_{52c4}, ζ_{52s4} in Eq. (4.19b) are obtained in a similar manner.

Using Eq. (A2.1) for y_c, the contribution of the third term in the first bracket of (A3.1) can be written

$$\frac{d\Gamma_{153}}{dt} = -\tfrac{1}{4}\bar{\Gamma}_{0y} B^2 r \int_0^\infty \frac{p}{\Omega(p)}[\{1 - \cos\Omega_p t\}\{\cos(\theta - \Omega_r t) - \cos(\theta + \Omega_r t) +$$

$$+ 2\Omega(r)t\mu[\sin(\theta + \Omega_r t) + \sin(3\theta - \Omega_r t)]\}]\, dp. \qquad \text{(A3.2)}$$

Again this may be integrated with respect to time by first setting $\theta = \theta_0 + \Omega_r t$ and treating θ_0 as a constant. The result is an expression of the form of Eq. (4.19c) where, for example,

$$\{\zeta_{53c}(r,t), \zeta_{53s}(r,t)\} = -\tfrac{1}{4}\bar{\Gamma}_{y0} B^2 tr \int_0^\infty (\chi_1, \chi_2)\frac{pdp}{\Omega(p)}$$

in which

$$\chi_1 = (1-\mu)\{\cos\Omega_r t - (\sin\Omega_r t)/\Omega_r t\} - \{\sin(\Omega_r + \Omega_p)t - \sin(\Omega_r - \Omega_p)t\}/(2\Omega_p t) +$$

$$+ (\tfrac{1}{2} - p_+)\{\sin(\Omega_r + \Omega_p)t + \sin\Omega_r t\}/\{(2\Omega_r + \Omega_p)t\} +$$

$$+ (\tfrac{1}{2} - p_-)\{\sin(\Omega_r - \Omega_p)t + \sin\Omega_r t\}/\{(2\Omega_r - \Omega_p)t\} +$$

$$+ p_+\cos(\Omega_r + \Omega_p)t + p_-\cos(\Omega_r - \Omega_p)t$$

and

$$\chi_2 = (1+\mu)\sin\Omega_r t + \{\cos(\Omega_r+\Omega_p)t - \cos(\Omega_r-\Omega_p)t\}/(2\Omega_p t) +$$
$$+ (\tfrac{1}{2} - p_+)\{\cos(\Omega_r+\Omega_p)t - \cos\Omega_r t\}/\{(2\Omega_r+\Omega_p)t\} +$$
$$+ (\tfrac{1}{2} - p_-)\{\cos(\Omega_r-\Omega_p)t - \cos\Omega_r t\}/\{(2\Omega_r-\Omega_p)t\} -$$
$$- p_+\sin(\Omega_r+\Omega_p)t - p_-\sin(\Omega_r-\Omega_p)t$$

where $p_+ = \mu\Omega_r/(2\Omega_r+\Omega_p)$ and $p_- = \mu\Omega_r/(2\Omega_r-\Omega_p)$. Expressions for ζ_{53c3} and ζ_{53s3} are obtained in a similar manner from the term proportional to $\sin(3\theta - \Omega_r t)$ in Eq. (A3.2).

References

Anthes, R. A. and Hoke, J. A. 1975 The effect of horizontal divergence and the latitudinal variation of the Coriolis parameter on the drift of a model hurricane. *Mon. Weather Rev.*, **103,** 757–763

Carr, L. E. and Williams, R. T. 1989 Barotropic vortex stability to perturbations from axisymmetry. *J. Atmos. Sci.*, **46,** 3177–3191

Chan, J. C. and Williams, R. T. 1987 Analytical and numerical studies of the beta-effect in tropical cyclone motion. Part I: Zero mean flow. *J. Atmos. Sci.* **44,** 1257–1265

DeMaria, M. 1985 Tropical cyclone motion in a nondivergent barotropic model. *Mon. Weather Rev.*, **113,** 1199–1210

1987 Tropical cyclone track prediction with a barotropic spectral model. *Mon. Weather Rev.*, **115,** 2346–2357

Fiorini, M. 1987 'The role of vortex structure in tropical cyclone motion'. Ph.D thesis, Naval Postgraduate School, Monterey, Calif., USA

Fiorino, M. and Elsberry, R. L. 1989a Some aspects of vortex structure related to tropical cyclone motion. *J. Atmos. Sci.*, **46,** 975–990

1989b Contributions to tropical cyclone motion by small, medium and large scales in the initial vortex. *Mon. Weather Rev.*, **117,** 721–727

Gent, P. R. and McWilliams, J. C. 1986 The instability of barotropic circular vortices. *Geophys. Astrophys. Fluid Dyn.*, **35,** 209–233

Holland, G. J. 1983 Tropical cyclone motion: environmental interaction plus a beta-effect. *J. Atmos. Sci.*, **40,** 328–342

Kasahara, A. 1957 The numerical prediction of hurricane movement with the barotropic model. *J. Meteorol.*, **14,** 386–402

1960 The numerical prediction of hurricane movement with a two-level baroclinic model. *J. Meteorol.*, **17,** 357–370

Kasahara, A. and Platzmann, G. W. 1963 Interaction of a hurricane with a steering field and its effect upon the hurricane trajectory. *Tellus*, **15,** 321–335

Kitade, T. 1981 Numerical experiments of tropical cyclones on a plane with variable Coriolis parameter. *J. Meteorol. Soc. Japan*, **58,** 471–488

Peng, M. S. and Williams, R. T. 1990 Dynamics of vortex asymmetries and their influence on vortex motion on a β-plane. *J. Atmos. Sci.*, **47,** 1987–2003

Sasaki, Y. 1955 Barotropic forecasting for the displacement of a typhoon. *J. Meteorol. Soc. Japan*, **32,** 1–8

Sasaki, Y. and Miyakoda, K. 1955 Numerical forecasting of the movement of a cyclone. *J. Meteorol. Soc. Japan*, **32,** 9–19

Shapiro, L. J. and Ooyama, K. V. 1990 Barotropic vortex evolution on a beta plane. *J. Atmos. Sci.*, **47,** 170–187

Smith, R. K. and Ulrich, W. 1990 An analytical theory of tropical cyclone motion using a barotropic model. *J. Atmos. Sci.*, **47,** 1973–1986

Smith, R. K., Ulrich, W. and Dietachmayer, G. 1990 A numerical study of tropical cyclone motion using a barotropic model. Part I: The role of vortex asymmetries. *Q.J.R. Meteorol. Soc.*, **116,** 337–362

Ulrich, W. and Smith, R. K. 1991 A numerical study of tropical cyclone motion using a barotropic model. Part II: Spatially-varying large-scale flows. *Q.J.R. Meteorol. Soc.*, **117,** 107–124

Weber, H. 1991 'The stability of barotropic vortices: implications for tropical cyclone motion.' Preprints of conference on Hurricanes and tropical meteorology, Miami, May 1991. American Meteorological Society

Willoughby, H. E. 1989 Linear motion of a shallow-water, barotropic vortex. *J. Atmos. Sci.*, **45**, 1906–1928